Time-responsive osteogenic niche of stem cells: A sequentially triggered, dual-peptide loaded, alginate hybrid system for promoting cell activity and osteo-differentiation

Zuyuan Luo [a, b], Siqi Zhang [b], Jijia Pan [b], Rui Shi [a], Hao Liu [a], Yalin Lyu [c, ***], Xiao Han [c], Yan Li [a], Yue Yang [d], Zhixiu Xu [e], Yi Sui [a], En Luo [f], Yuanyuan Zhang [g, **], Shicheng Wei [a, b, *]

[a] Central Laboratory, School and Hospital of Stomatology, Peking University, National Engineering Laboratory for Digital and Material Technology of Stomatology, Beijing 100081, China
[b] Laboratory for Biomaterials and Regenerative Medicine, Academy for Advanced Interdisciplinary Studies, Peking University, Beijing 100871, China
[c] Department of Stomatology, Beijing Anzhen Hospital, Capital Medical University, Beijing 100029, China
[d] Department of Stomatology, Xuanwu Hospital, Capital Medical University, Beijing 100053, China
[e] Department of Oral Pathology, School and Hospital of Stomatology, Peking University, Beijing 100081, China
[f] Department of Oral and Maxillofacial Surgery, West China School and Hospital of Stomatology, Sichuan University, Chengdu 610041, China
[g] Wake Forest Institute for Regenerative Medicine, Wake Forest School of Medicine, Winston-Salem, NC 27157, USA

ARTICLE INFO

ABSTRACT

The efficacy of stem cell-based bone tissue engineering has been hampered by cell death and limited fate control. A smart cell culture system with the capability of sequentially delivering multiple factors in specific growth stages, like the mechanism of the natural extracellular matrix modulating tissue formation, is attractive for enhancing cell activity and controlling cell fate. Here, a bone forming peptide-1 (BFP-1)-laden mesoporous silica nanoparticles (pep@MSNs) incorporated adhesion peptide, containing the arginine-glycine-aspartic acid (RGD) domain, modified alginate hydrogel (RA) system (pep@MSNs-RA) was developed to promote the activity and stimulate osteo-differentiation of human mesenchymal stem cells (hMSCs) in sequence. The survivability and proliferation of hMSCs were enhanced in the adhesion peptide modified hydrogel. Next, BFP-1 released from pep@MSNs induced hMSCs osteo-differentiation after the proliferation stage. Moreover, BFP-1 near the cells was self-captured by the additional cell-peptide cross-linked networks formed by the ligands (RGD) binding to receptors on the cell surface, leading to long-term sustained osteo-stimulation of hMSCs. The results suggest that independent and sequential stimulation in proliferation and osteo-differentiation stages could synergistically enhance the survivability, expansion, and osteogenesis of hMSCs, as compared to stimulating alone or simultaneously. Overall, this study provided a new and valid strategy for stem cell expansion and osteo-differentiation in 2D or 3D culture systems, possessing potential applications in 3D bio-printing and tissue regeneration.

1. Introduction

Stem cell-based tissue engineering holds great clinical promise. Guiding stem cells to differentiate into a specific cell type is the most important step for successful cell therapy [1] because stem cells may otherwise differentiate into unwanted cells or tissues, including tumors [2,3]. Material-based matrixes and bio-factors are the two most important elements for guiding stem cell differentiation [3–5]. For bone tissue regeneration, biophysical and biochemical cues from extracellular matrix (ECM) such as stiffness, topography, and porosity, as well as binding functional groups have

been reported to control stem cell differentiation [6—9]. Also, many bio-factors including β-glycerol phosphate, dexamethasone, and various growth factors (including bone morphogenetic proteins [BMPs]) have been developed [10—13]. However, most of these strategies typically rely on only a single differentiation factor to induce osteogenic differentiation (osteo-differentiation) and neglect to enhance the survival and proliferation of cells, which may partially mimic the native microenvironment and hamper tissue regeneration.

Importantly, cell survival and proliferation are important events preceding cell differentiation [14,15], and the osteo-differentiation is based on the extent of cell-cell contact [16]. The cells regard each other as their surrounding "microenvironment", and thus the biomechanical or biochemical cues from neighboring cells represent a way of stimulating osteo-differentiation [17—19]. Tang et al. found that the extent of osteo-differentiation was fairly linearly related to the extent of neighboring cells [16]. Moreover, cell therapy is based on a large number of cells, and therefore requires enough time for cell expansion before differentiation. In addition, increasing efforts have demonstrated that incorporated biological signals should be presented at the right time and right place [20]. Thus, the desired material-based matrix for cell therapy should hold the ability to bind, store, and deliver growth factors in the appropriate growth stage [21], which could provide a stimulatory environment for stem cell expansion and differentiation in sequence. Mooney et al. developed a dual delivery system for vascular endothelial growth factor (VEGF) and platelet-derived growth factor (PDGF)-BB from a structural polymer scaffold, resulting in the rapid formation of a mature vascular network [22]. Delivery of these molecules in tandem elicited synergistically enhanced vessel formation, whereas VEGF or PDGF-BB delivery alone resulted in fragile vascularity or no significant vessel formation [22]. For bone tissue engineering, some studies have attempted to achieve the goal by simultaneously bonding integrin binding ligands (such as vitronectin or laminin) and osteoinductive growth factors (including BMP-7) to promote osteo-differentiation of hMSCs or human embryonic stem cells [23—25]. To date, the most challenging aspect in these studies is sequentially presenting appropriate factors during specific growth stages. Thus, in this study, we explored a facile and versatile dual-peptide loaded alginate-based hydrogel system to deliver growth factors in specific stages, which is similar to the mechanism of the natural ECM where modulation of tissue formation occurs. Using this system, the activity and proliferation of stem cells was enhanced first, and then osteo-differentiation was markedly induced.

Alginate has been widely used in numerous biomedical applications including tissue regeneration, drug delivery and cell encapsulation [26,27], for its high biocompatibility, low toxicity and relatively low cost. Nevertheless, alginate is a flexible polymer that presents no cell adhesion ligands, resulting in a low cell survival rate. Typically, integrin binding ligands, such as RGD peptides, are coupled to alginate polymer chains to enhance cell viability and promote cell proliferation [28—30]. Bone morphogenetic proteins, including BMP-2, BMP-4, and BMP-7, are the most potent osteo-inductive growth factors [24,25]. A peptide derived from the immature region of BMP-7, which has higher osteogenesis activity than BMP-7 [31,32], named bone forming peptide-1 (BFP-1), was employed to induce the osteo-differentiation of hMSCs. In this system, BFP-1 should be stored in a reservoir and delivered in a controlled and sustained manner. Mesoporous silica nanoparticles (MSNs) with large surface areas, adjustable pore sizes and high biocompatibility, have been extensively studied as nanoscale drug delivery carriers [33—35]. Overall, BFP-1 was incorporated into MSNs to obtain the peptide-

laden MSNs (pep@MSNs), and then the pep@MSNs were encapsulated into the RGD-treated alginate hydrogel (RA) to form pep@MSNs-RA.

In this niche, the activity of hMSCs is first promoted by the RGD peptide (proliferation factor). Thereafter, the BFP-1 (osteogenesis factor) released from the pep@MSNs induces hMSCs osteo-differentiation after cells expansion and the formation of cell-cell contacts. Moreover, Mooney et al. reported that the cell-polymer interactions would be formed by the ligands binding to receptors on the cell surface [36]. BFP-1 around the cells could be captured by the additional cell-peptide cross-linked networks, leading to long-term sustained osteo-stimulation of hMSCs (Fig. 1). In this study, we tested the hypothesis that independent and sequential stimulation in the proliferation and osteogenesis stages can synergistically enhance the survivability, expansion and osteo-differentiation of hMSCs, compared to stimulation alone or simultaneously. The time-responsive cell culture system provides a niche-like native ECM for stem cell survival and growth into mature bone tissue, with potential applications in tissue engineering and organoids culture.

2. Experimental section

2.1. Materials

Sodium alginate (SA) with high mannuronic acid content (G/M ≈ 0.64) and calcium sulfate powders were purchased from Sigma-Aldrich (St. Louis, USA). 2-(N-morpholino) ethanesulfonic acid (MES), N-hydroxy-sulfosuccinimide (sulfo-NHS), and 1-(3-dimethylaminopropyl)-3-ethylcarbodiimide (EDC) were obtained from Aladdin Reagent Co. Ltd. (Shanghai, China). The RGD peptide (GGGGRGDASSP sequence), fluorescein isothiocyanate (FITC)-labeled RGD, BFP-1 (GQGFSYPYKAVFSTQ sequence), and the 6-carboxy tetramethyl rhodamine-labeled (TAMRA-labeled) BFP-1 were purchased from ChinaPeptides Co. Ltd. (Shanghai, China) and all the peptides were synthesized by a batch-wise fmoc-polyamide method to achieve greater than 98% purity. All other chemicals were of analytical reagent grade and used as received unless noted. All aqueous solutions were prepared with deionized water.

2.2. Fabrication of pep@MSNs

The preparation of MSNs and BFP-1 laden MSNs (pep@MSNs) was performed as previously described [33]. Briefly, 100 mg of the solid material was immersed in 10 mL of 10^{-4} mol L^{-1} BFP-1 (or TAMRA-labeled BFP-1) solution (in phosphate-buffered saline [PBS]) with stirring for 30 min. Subsequently, the BFP-1 (or TAMRA-labeled BFP-1) laden MSNs were washed with deionized water three times to remove excess non-adsorbed peptide, and dried at ambient temperature.

2.3. Preparation of alginate hydrogels

The adhesion peptide that contains the RGD sequence was utilized to promote hMSCs adhesion, spreading, and proliferation. RGD peptide was coupled to alginate polymers using published carbodiimide chemistry [28]. Briefly, EDC and sulfo-NHS were reacted with alginate solution in MES buffer to form a stable intermediate, and RGD was added to the solution and allowed to react overnight at room temperature. The concentration of peptides and polymer was 20 peptides per polymer chain, and the efficacy of peptides coupled to alginate was characterized using FITC-labeled RGD peptides. Following peptides treatment, alginate was dialyzed (3.5 kDa), sterile filtered (0.22 μm), and freeze-dried.
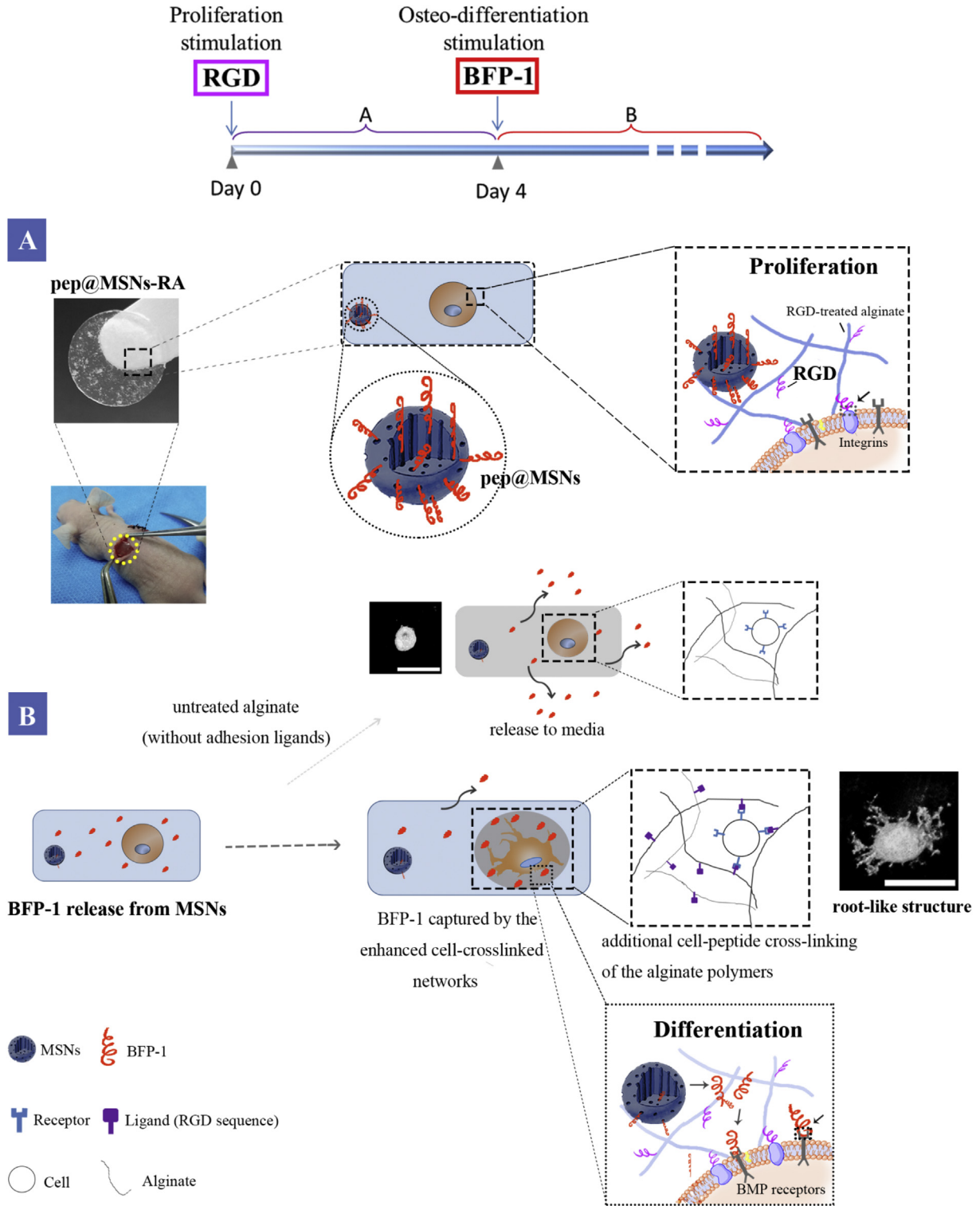
Fig. 1. Schematic illustration of pep@MSNs-RA with the independent and sequential dual-peptide delivery system for promoting the proliferation and osteo-differentiation of mesenchymal stem cells. Scale bar: 50 μm.

To prepare UA and RA, calcium sulfate slurry (1.22 M in deionized water) was mixed with 2% (wt) solutions of untreated (or RGD-treated) alginate using Luer lock syringes, and crosslinked between two glass plates separated by a spacer (2 mm). After hydrogel matrixes were crosslinked for 45 min, discs that were 2 mm in thickness and 14 mm in diameter were punched out with a metal dye.

The pep@MSNs-RA was formed by the same method as RA. Based on the various concentrations (0.5, 1.0, 1.5 and 2.0 mg L^{-1}) of pep@MSNs powders in the alginate solution, the hydrogel matrixes were respectively named as 0.5pep@MSNs-RA, 1.0pep@MSNs-RA, 1.5pep@MSNs-RA and 2.0pep@MSNs-RA, respectively (Table S1).

Typically, BFP-1 was introduced to RGD-treated alginate hydrogel in two ways as control groups. As shown in Table S1, to form BFP-1 peptide incorporated RA (pep-RA), free BFP-1 (5 µg per 1 mL alginate solution) was mixed with RGD-treated alginate solution without carbodiimide treatment. In addition, before preparation of BFP-1, RGD-treated alginate hydrogel (PRA), the BFP-1, RGD-treated alginate was synthesized. BFP-1 (5 µg per 1 mL alginate solution) and RGD peptides were coupled to the alginate polymers using the same published carbodiimide chemistry as described in the previous section.

2.4. Characterization of MSNs and functional alginate hydrogels

The ordered mesoporous structure of MSNs was confirmed by transmission electron microscope (TEM; Tecnai F20, Philips, Netherlands). The release profiles of BFP-1 peptide from pep@MSNs-RA, PRA and pep-RA were assessed using TAMRA-labeled BFP-1 peptides. Each matrix was immersed in 10 mL of PBS (pH 7.4, 37 °C) for up to 52 days, respectively. At the predetermined time points, 100 µL of supernatant was collected for calculation of the peptide released in solution using the fluorescence microplate reader (SpectraMax M5, Molecular Devices, USA). The concentration of peptide was calculated by comparison with the established standard curve. For elastic modulus measurement, alginate hydrogel matrixes (14 mm diameter and 2 mm thickness) were subjected to an unconfined compression test (1 mm/min) in a mechanical apparatus (ElectroForce 3100, BOSE, USA), immediately after being cast or after swelling to equilibrium in media for a predetermined time at 37 °C. The surface hydrophilicity was measured by water contact angle goniometry (SL200B, Kono, USA).

2.5. Cells culture and seeding on 2D matrixes

hMSCs were purchased from ScienCell Research Laboratories (Carlsbad, CA, USA) and maintained in low glucose Dulbecco's modified Eagle medium (DMEM; Hyclone, USA) supplemented with 10% fetal bovine serum (Gibco, NY, USA) and 1% penicillin/streptomycin (Gibco), and used between passages 4–5. The cell-peptide crosslinked networks were demonstrated by adding soluble RGD peptide to block the adhesion with matrixes [29]. Briefly, hMSCs were co-cultured with the media with soluble RGD (1 mM) for 12 h before being encapsulated. These cells were named RGD-blocked hMSCs (b-hMSCs).

For 2D cell culture on hydrogels, hMSCs were seeded in 24-well plates (Costar, USA) with different alginate hydrogel substrates at a density of 2×10^4 cells per well. The culture media was then changed to the osteogenic differentiation media (low glucose DMEM supplemented with 10 mM β-glycerol phosphate, 50 µg mL^{-1} ascorbic acid and 0.1 µM dexamethasone; all from Sigma-Aldrich). The cells were cultured under a 5% CO_2 atmosphere at 37 °C and the medium (1.5 mL/well) was changed every three days.

2.6. Cells in 3D matrixes culture

For alginate-based 3D culture studies, hMSCs in flasks were trypsinized using 0.05% trypsin/EDTA (Gibco), washed once in serum-free low glucose DMEM, and resuspended in the same serum-free media at 10 × the final concentration. Subsequently, cell suspensions were mixed well with different alginate solutions (Table S1) using Luer-lock syringes and a female-female Luer lock coupler. The cell-alginate solutions (1.0×10^7 cells/mL in alginate) were then rapidly mixed with low glucose DMEM containing the appropriate concentration of calcium sulfate (1.22 M in DMEM), and then deposited between two glass plates spaced 1 mm apart.

The solutions were allowed to gel for 30 min, and then disks of hydrogel (14 mm diameter and 1 mm thickness) were punched out and transferred to 24-well plates (Costar) where they were immersed in 1.5 mL osteogenic differentiation media.

2.7. Proliferation of hMSCs in 2D or 3D culture systems

The cell counting kit-8 assay (CCK-8, Dojindo, Japan) was used to evaluate the viability of cells grown in both 2D and 3D systems. Briefly, after incubation for 1, 3, 7, and 14 days, 150 µL of CCK-8 was added into each well for 3 h, and the absorbance value of the supernatant optical density (OD) was measured with a microplate reader (SpectraMax M5) at 450 nm. In addition, 2×10^4 cells in 1.5 mL DMEM medium (containing 10% dimethyl sulfoxide) were added into empty wells as a positive control. Furthermore, hMSCs viability within multi-component 3D hydrogel matrixes after 8 h of culture was qualitatively assessed with a live/dead staining kit (Dojindo) following the manufacturer's instructions.

2.8. Morphologies and cytoskeletal observation

The morphology of cells cultured on 2D matrix was examined by obtaining scanning electron microscope (S-4800, Hitachi, Japan) sections of specimens that were flash-frozen in liquid nitrogen and freeze-dried. The cytoskeleton of hMSCs in both the 2D and 3D systems was observed by confocal laser scanning microscopy (CLSM; A1R-si, Nikon, Japan). For CLSM observation, hydrogel matrixes were washed with PBS and fixed with 4% (w/v) paraformaldehyde (Hyclone) for 30 min. The samples were then permeabilized with 0.5% (v/v) Triton X-100 (Sigma-Aldrich) for 15 min, and stained with 5 µg mL^{-1} FITC-phalloidin solution (Sigma) for 30 min. After being washed with PBS, samples were incubated for 10 min at room temperature with 10 µg mL^{-1} 4′,6-diamidine-2-phenylindole (DAPI) solution (Sigma-Aldrich).

2.9. Cells extraction for alkaline phosphatase (ALP) and RNA analysis

To analyze ALP and osteo-related RNA expression, cells were extracted from both 2D and 3D culture gels. Typically, media was removed from the gels first, and then the gels were placed directly in 5 mL of cooled PBS with 50 mM ethylenediaminetetraacetic acid (EDTA) on ice. The mixture was pipetted and vortexed periodically to disassociate the gels, centrifuged to separate a pellet of cells from the EDTA solution, and the supernatant was removed. For analysis of RNA expression, the cells were washed again, and the pellet was lysed with TRIzol reagent (Invitrogen, USA) and converted to cDNA using a Revert Aid First Strand cDNA Synthesis Kit (Thermo, USA). Quantitative real-time PCR (Q-PCR) analysis was carried out with SYBR Green (Roche, USA) on an ABI 7500 RT-PCR machine (Applied Biosystems, USA). β-actin mRNA was used as an internal control for PCR amplification. Primers (5′–3′) used in this study are listed in Table S2. Primer sets (10 µM final concentration for each primer) were used in a volume of 20 µL per tube. The thermal profile of the PCR was 50 °C for 2 min, 95 °C for 10 min, followed by 40 cycles at 95 °C for 15 s and 60 °C for 1 min. The comparative CT ($2^{-\Delta\Delta CT}$) method was employed to evaluate gene expression differences between groups.

For quantitative analysis of ALP expression, the cell pellet was resuspended in 1% Triton X-100 (v/v) for 1 h. The cell-lysis solution was then collected and centrifuged (12,000 rpm, 4 °C) for 30 min to remove all cell debris. Afterwards, 30 µL of the supernatant was transferred to a new 96-well plate for ALP determination

according to the manufacturer's instructions (Nanjing Jiancheng Biotechnology, China). For normalization, the total protein concentration was measured by a bicinchoninic acid (BCA) protein assay kit (Pierce 23227, Thermo, USA). The in situ staining for ALP was visualized using the BCIP/NBT ALP color development kit (Beyotime, China) following the manufacturer's instruction.

2.10. Immunofluorescence

After 7 or 14 days of culture, cells grown in both 2D and 3D systems were fixed with paraformaldehyde (4%) for 30 min and permeabilized with Triton X-100 (0.1%) for 15 min at 25 °C. After washing three times with PBS, cells were incubated with 3% bovine serum albumin solution (Sigma-Aldrich) for 2 h at 37 °C to block nonspecific binding. Afterwards, cells were incubated with primary antibodies (mouse polyclonal antihuman integrin β1 [1:200, Abcam, UK], rabbit monoclonal antihuman osteocalcin [OCN, 1:100, Abcam, UK], mouse polyclonal antihuman Collagen I [Col1a1, 1:100, Abcam] and rabbit monoclonal antihuman Runx2 [1:100, Abcam]), at 4 °C overnight. Cells were then washed three times with PBS and incubated with secondary antibodies at a dilution of 1:1000 for 1 h in the dark at room temperature (FITC-X goat anti-rabbit IgG and Rhodamine Red^{TM}-X goat anti-mouse IgG, Invitrogen, USA). Finally, cell nuclei were stained with DAPI for 10 min at room temperature. The stained signals in the cells were visualized immediately by CLSM.

2.11. Protein extraction and western blot analysis

After 14 days of culture, alginate matrixes were washed with Dulbecco's PBS (dPBS), then immersed in 5 mL of dPBS with 50 mM EDTA. Cells were pelleted and lysed with RIPA buffer (Sigma-Aldrich) with proteinase inhibitor (Roche, Switzerland) on ice for 30 min. Protein content of lysates was determined with the BCA protein assay kit. The proteins were separated by sodium dodecyl sulfate-polyacrylamide gel electrophoresis and transferred to polyvinylidene fluoride membranes (Millipore, USA). Membranes were blocked with skim milk (5%) in TBST for 1 h, and then incubated with the primary antibodies OCN (1:1000, Abcam) and Col1a1 (1:1000, Abcam) overnight at 4 °C. The bands were then visualized after incubation for 1 h with horseradish peroxidase (HRP)-conjugated secondary antibodies by chemiluminescence using an ECL detection kit (Amersham). β-actin was used as an internal control.

2.12. Subcutaneous implantation in nude mice

For the in vivo study, we chose a murine dorsal subcutaneous pocket model to estimate the bone formation of different matrixes encapsulated with hMSCs. The encapsulation of hMSCs into UA, RA, pep-RA, and pep@MSNs-RA referred to the above method. Briefly, hMSCs were encapsulated into different alginate-based aqueous solutions using Luer-lock syringes and a female-female Luer-lock coupler. The cell-alginate solutions (1.0×10^7 cells/mL in alginate) were then rapidly mixed with calcium sulfate, and then deposited between two glass plates spaced 1 mm apart. The solutions were allowed to gel for 30 min, and then disks of hydrogel (5 mm diameter) were punched out and maintained in media for 24 h before implantation. All animals described in the present study were reviewed and approved by the Animal Care and Use Committee of Peking University. Female BALB/c nude mice (6—8 weeks) separately implanted with matrixes for assessing the osteo-differentiation. After mice were anesthetized by intraperitoneal injection of sodium pentobarbital (70 μg/g), two independent incisions were created subcutaneously on the back of each mouse.

Every mouse received four subcutaneous implants containing UA, RA, pep-RA, and pep@MSNs-RA, and the implants were allowed to develop in vivo for 2 and 4 weeks.

2.13. Histological and micro-CT analysis

After mice were euthanized 2 weeks (n = 6) and 4 weeks (n = 6) post-surgery, samples were excised and fixed overnight in 10% neutral formalin (Solarbio, China). Total bone volume formed in gels at both 2 and 4 weeks was visualized and quantified using micro-computed tomography (micro-CT). The samples was imaged (60 kV, 0.22 mA, 60 s) using a high resolution micro-CT specimen scanner (Inveon MM CT, SIEMENS). And the explant bone volume was measured by Inveon Research Workplace software (SIEMENS, USA). A threshold (1000—4500 mg HA/cc) was determined subjectively from the reconstructed images to partition mineralized tissue from fluid and soft-tissues. Afterwards, the samples were processed for paraffin sections, and the sections (5 μm) were processed for hematoxylin and eosin (H&E) staining, Masson's trichrome (MT) staining, Alizarin Red S (ARS) staining, and immunohistochemistry (IHC) staining. For IF staining, samples were embedded in optimal cutting temperature compound (Sakura Finetek, Japan) and sliced into 15 μm thick sections. The primary antibodies for IHC and IF staining, including Col1a1 (ab90395), OCN (ab13418) and OPN (ab69498), were all purchased from Abcam and did not react with mouse.

2.14. Statistical analysis

All data were expressed as the mean $\pm$ standard deviation of a representative three experiments. Statistical analysis was performed by one-way analysis of variance (ANOVA) followed by Tukey's post hoc tests using SPSS 19.0 and p-values less than 0.05 were considered statistically significant.

3. Results and discussion

3.1. Preparation and characterization of pep@MSNs-RA

Alginate is a block copolymer composed of regions of sequential mannuronic acid units and guluronic acid units (M-blocks and G-blocks, respectively), and the G-blocks can be cross-linked by divalent cations such as calcium (Ca^{2+}) [26]. In this study, hydrogels were prepared by mixing alginate solutions with calcium sulfate slurry [37]. However, alginate is a flexible polymer that presents no intrinsic cell adhesion ligands, resulting in a low cell adhesion and survival rate [38]. An adhesion peptide (GGGGRGDASSP) with an RGD sequence was coupled to alginate polymers to create integrin-binding ligands using published carbodiimide chemistry [28]. The coupling efficiency used in this procedure was qualitatively characterized using FITC-labeled RGD (FITC-RGD). From CLSM images, the uniform fluorescence (green) distribution was observed in RA (Fig. S1), signifying the homogeneity of FITC-RGD conjugated in the hydrogel. Simultaneously, the BFP-1 peptide-laden nanoparticles (pep@MSNs) were synthesized by our previously reported protocol [33]. Subsequently, pep@MSNs were added into the RGD-treated alginate solution by adequate mixing and then these hybrids were mixed with the calcium sulfate slurry (1.22 M) to form multi-phase pep@MSNs-RA (Fig. 2A and B). Based on the different concentrations of pep@MSNs in the gels, the prepared specimens were denoted as (0.5, 1.0, 1.5, or 2.0)pep@MSNs-RA (Table S1). In contrast, BFP-1 was mixed with RGD-treated alginate solution with or without carbodiimide treatment to form pep-RA or PRA, respectively (Table S1).

The elastic modulus of hydrogel matrixes is very significant to
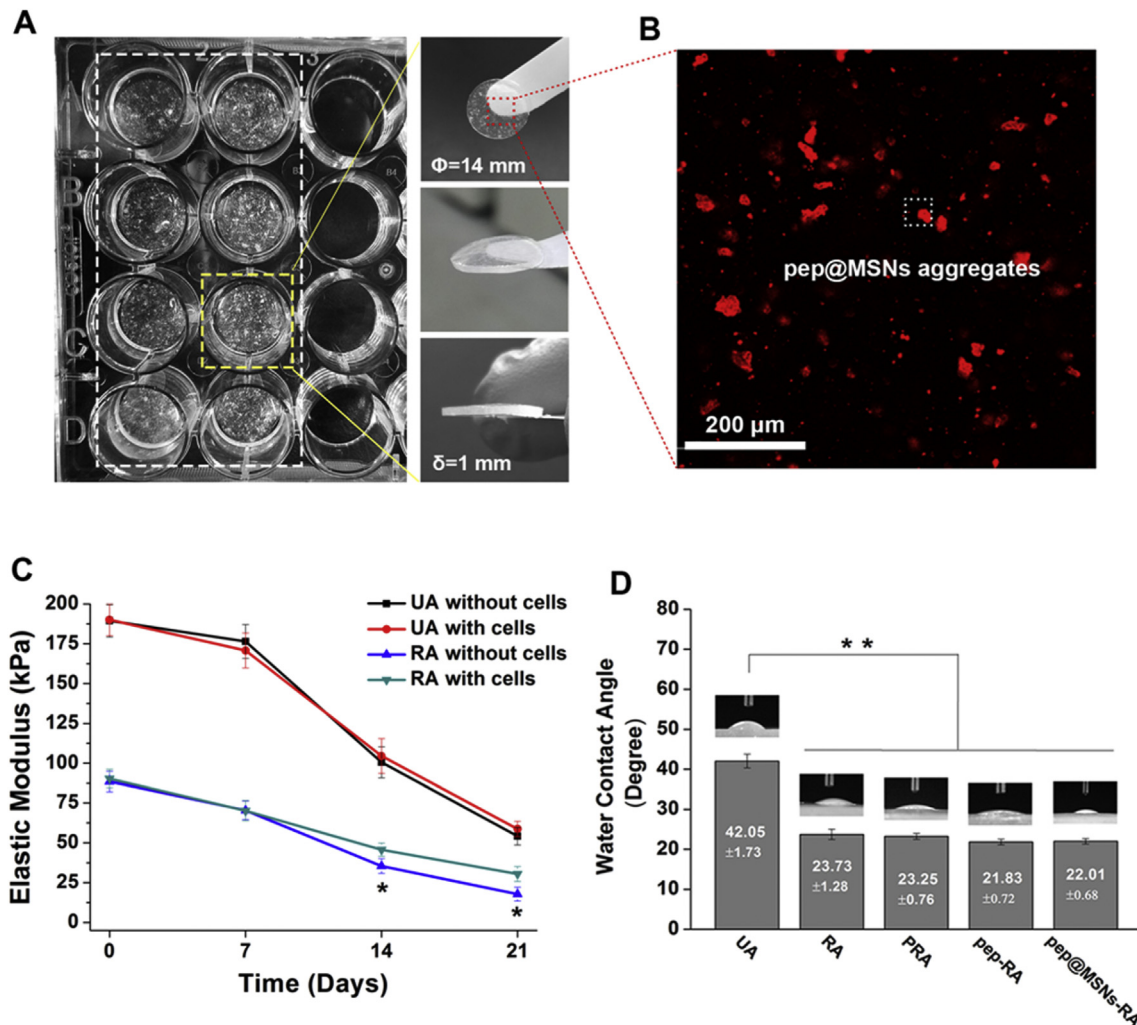
Fig. 2. Fabrication and characterisation of pep@MSNs-RA. A) Photographs of pep@MSNs-RA matrixes. B) Confocal laser scanning microscopy (CLSM) image of TAMRA-labeled pep@MSNs aggregates. C) The elastic modulus of untreated or RGD-treated alginate gels with or without cells encapsulated changing with time, respectively. D) Water contact angle of specimens, and the insets present the water droplet pictures of each sample. The p value was calculated by Tukey's post-hoc test ($^*p < 0.05$ and $^{**}p < 0.01$). All data represent mean $\pm$ SD ($n = 3$).

stem cell survival and differentiation [38–40]. Alginate ligand density, polymer and cross-linker concentrations can be used to modulate hydrogel stiffness [37]. The compression test results showed that the untreated UA has an initial elastic modulus of 190 kPa, however, the RA based gels (including RA, PRA, pep-RA, and pep@MSNs-RA) were about 90 kPa (Fig. S2). The divalent cations are believed to bind solely to G-blocks of alginate chains, thus the mechanical properties of ionically cross-linked alginate gels can vary significantly depending on the content of the guluronate residues [26]. The lower stiffness in RA based gels could be attributed to the decreased density of carboxylic groups in G-blocks that were swallowed by RGD peptides [40]. However, there were no obvious differences among RA, PRA, pep-RA and pep@MSNs-RA, demonstrating that hydrogel stiffness would not be affected by incorporation of BFP-1 or pep@MSNs. Additionally, these matrixes were immersed in media for 14 and 28 days to measure the change in the elastic modulus over time. Such Ca^{2+} cross-linked alginate hydrogels were stable over a timescale of at least 14 days under tissue culture conditions (Fig. S2), providing an ECM for cell growth. However, the higher elastic moduli were found in the RA with cell-encapsulated groups after culturing in media for 7 days (Fig. 2C). The additional mechanical integrity of

the gels could be due to the formation of cell-RGD peptide cross-linked networks, via binding interactions between cells and the ligands coupled to the alginate chains [36]. In previous reports, the additional networks could cause prolonged release of drugs incorporated in hydrogels [41].

Moreover, the water contact angle (WCA) on a substrate has been widely used to track and evaluate the effectiveness of modification protocols, as it can provide information on the wettability and surface energy of biomaterials. Strikingly, the WCA on the UA after RGD coupling decreased from $42.05 \pm 1.73°$ to $23.73 \pm 1.28°$, while no statistical difference could be found among RA, PRA and pep-RA (Fig. 2D and inset). Such significant changes in surface hydrophilicity could be due to the super-hydrophilic property of bonded RGD peptides and might impact the attachment of hMSCs [42].

3.2. Drug release behaviors of pep@MSNs-RA

The release profiles of BFP-1 from pep-RA, PRA, 0.5, 1.0, 1.5, and 2.0pep@MSNs-RA were studied. Fig. 3A displayed that a very small fraction of peptide (less than 1%) was released from PRA in the first 22 days, while an abrupt increase in the amount of released
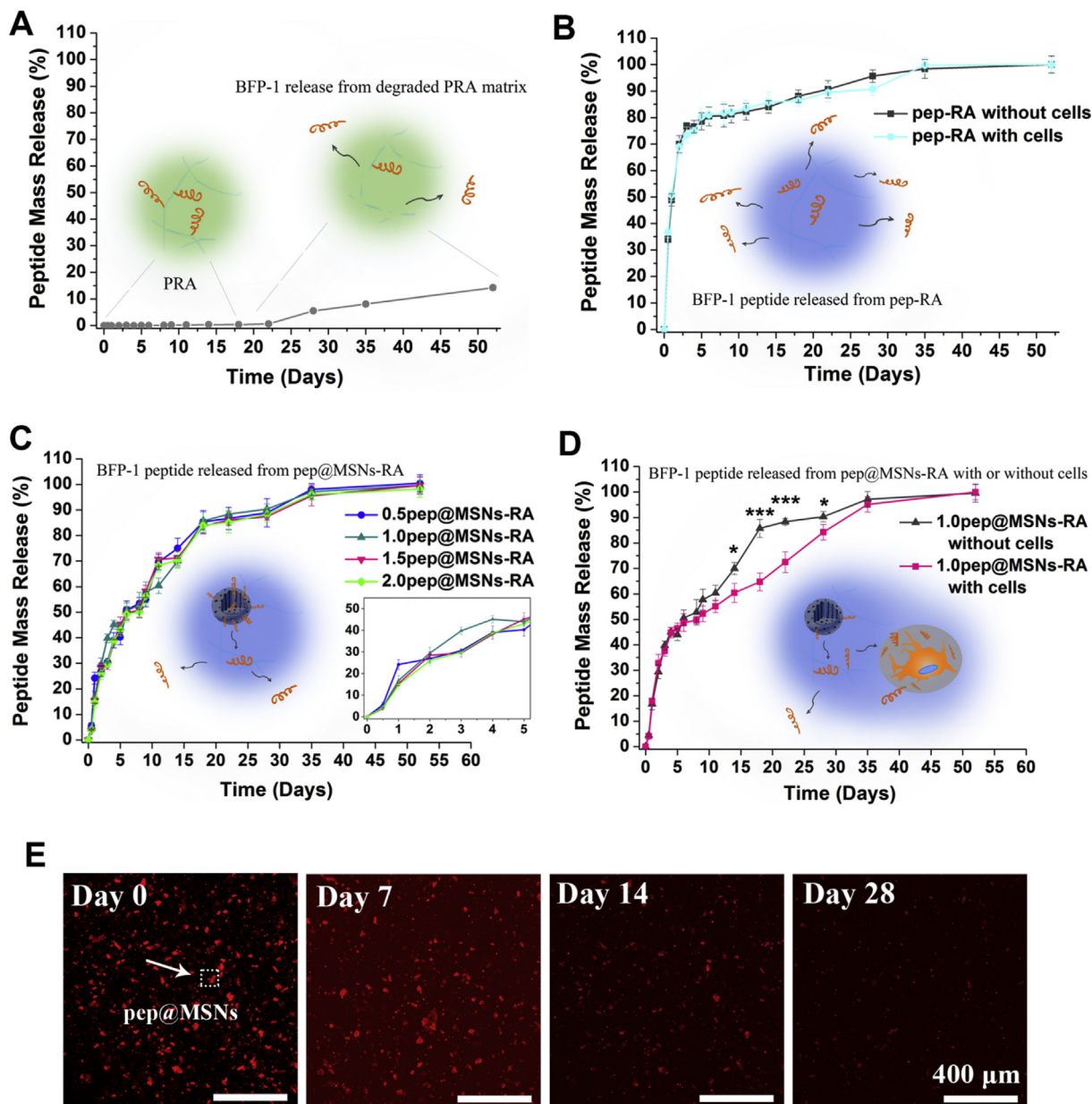
Fig. 3. Bone forming peptide-1 (BFP-1) release behavior from different matrixes. BFP-1 release profiles A) from PRA, B) from pep-RA with or without cells encapsulated, C) from pep@MSNs-RA with different incorporated pep@MSNs concentrations (without cells), and D) from pep@MSNs-RA with or without encapsulated cells. E) The fluorescence retained by the pep@MSNs-RA gel over a long incubation period (28 days). TAMRA-tagged BFP-1 used for the fluorescence intensity measurement during incubation. The *p* value was calculated by Tukey's post-hoc test (*$p < 0.05$ and ***$p < 0.001$). All data represent mean ± SD ($n = 3$).

peptide was found after day 23. As said in the prepare protocol of PRA, BFP-1 was covalently coupled to alginate using the carbodiimide chemistry method, which resulted in stable binding between BFP-1 and alginate. Bulk degradation of PRA after the day 23 could lead to BFP-1 escaping from PRA. However, the pep-RA release profiles (Fig. 3B) showed an initial burst release of 50—60%, and more than 80% of the total peptide amount was released into the media on the 4th day. Almost all BFP-1 was released into the media before formation of the cell-peptide cross-linked networks. No significant difference was found after hMSCs were encapsulated into pep-RA (Fig. 3B). The BFP-1 release profiles of all pep@MSNs-RA families (without cells) exhibited a long-term sustained delivery behavior (Fig. 3C). An approximately 50% dose of peptide was released in a relatively sustained rate in the first 6 days, and about

70% of the total laden peptide was delivered on the day 14. The fluorescence (TAMRA-BFP-1) retention images of pep@MSNs-RA were also captured during incubation for long periods of up to 28 days (Fig. 3E). The fluorescence intensity decreased very slowly, suggesting a high retention of BFP-1 in the nanocarrier-encapsulated gels. Such favorable release could be attributed to the excellent drug delivery capacity of MSNs. In our previous study, the peptide-laden MSNs (pep@MSNs) showed a sustained peptide release pattern and lasted for more than 7 days [33]. MSNs contain plenty of uniform and homogeneous pore channels (Fig. S3), giving the opportunity for MSNs to be applied as an excellent drug carrier. The favorable incorporation of BFP-1 (about 7.0×10^{-6} mol peptide laden in 1 g MSNs, Fig. S4) may be due to the hydrogen bonding or long-range electrostatic ionic amine bonds ($Si{-}O^{-}{-}{^{+}}H_3N$) formed
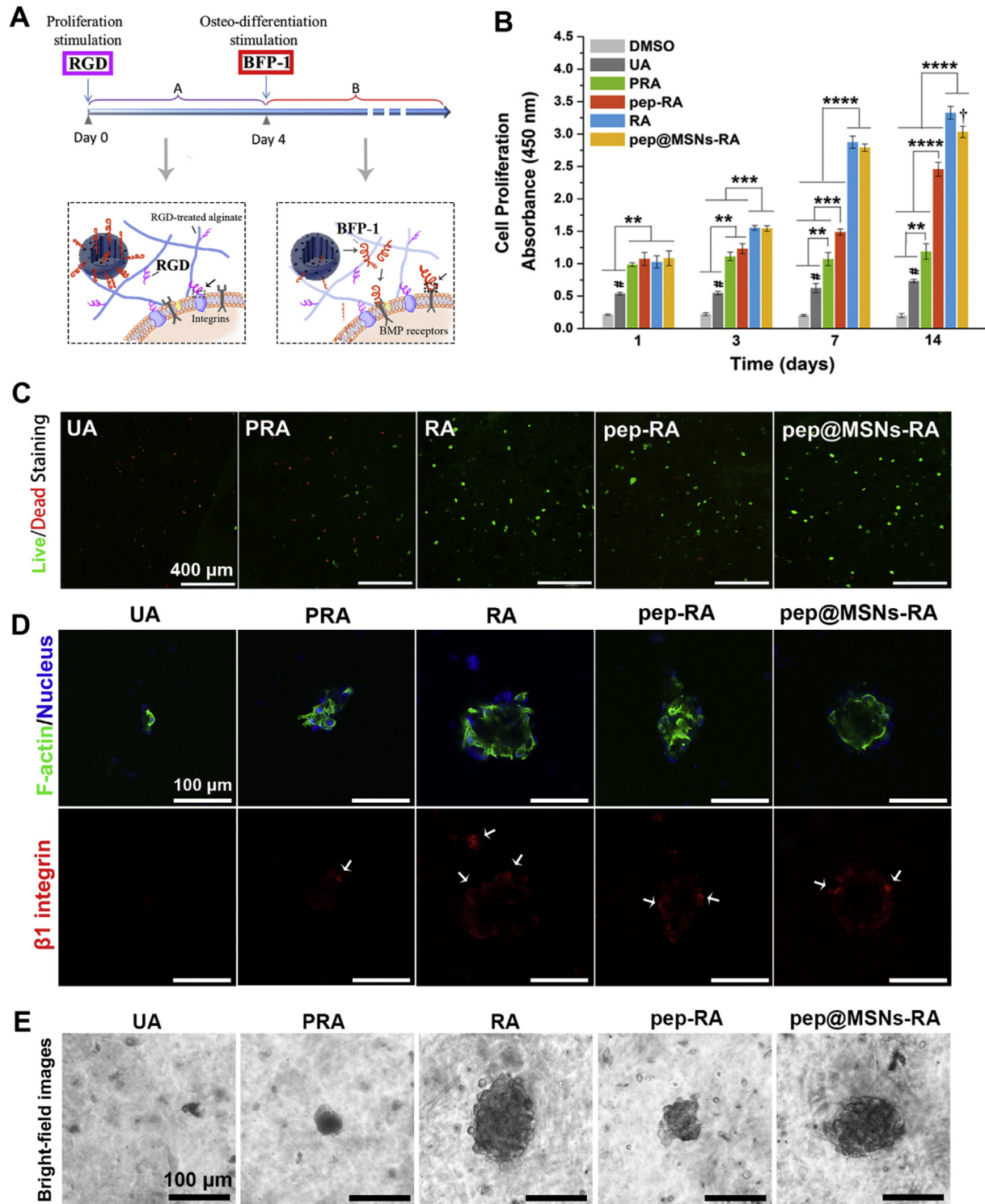
Fig. 4. The survival and proliferation of hMSCs encapsulated in different 3D matrixes. A) Illustration of the dual-peptide loaded alginate-based hybrid system sequentially promoting the proliferation and inducing osteo-differentiation of hMSCs. B) Proliferation of hMSCs 3D cultured in different matrixes for 1, 3, 7 and 14 days. C) Representative live/dead stainning images of hMSCs encapsulated in various gels for 5 days. D) *In situ* immunofluorescence staining for F-actin and integrin β1 in hMSCs encapsulated in various gels at day 7. E) Bright-field images of hMSCs clusters in various gels at day 7. The *p* values were calculated by Tukey's post-hoc test (**$p < 0.01$, ***$p < 0.001$, and ****$p < 0.0001$; †$p < 0.01$, relative to pep-RA and pep@MSNs-RA). All data represent mean ± SD ($n = 3$).

between the silanol group present in the MSNs and the *N*-terminal side chains of the Gln, and Thr amino acids or the amino group of the first Ala [43,44].

Furthermore, slower delivery of BFP-1 was found in the pep@MSNs-RA with the cell-encapsulated group after incubation for two weeks (Fig. 3D). As shown in Fig. S5, pep@MSNs-RA delivered BFP-1 in a cell-dose-dependent manner, where the pep@MSNs-RA with higher cell concentration exhibited a slower

release performance for BFP-1. However, a statistical difference was found between pep@MSNs-RA encapsulated with hMSCs and b-hMSCs (2×10^7 cells/mL) after two weeks (Fig. S5). b-hMSCs were co-cultured with soluble RGD peptide before encapsulation in the matrix and the soluble RGD could block the cell-material cross-linking [29]. These results demonstrated that the prolonged release of BFP-1 was due to the additional cell-peptide cross-linked networks [41,45], which was supported by the stiffness test and was in accordance with test results.

Moreover, the amount of peptide released in the media was measured based on the results in Fig. S4. As shown in Table S3, $1.12 \pm 0.04 \, \mu g \, mL^{-1}$ of BFP-1 was released into media from pep-RA after 12 h, which could induce osteo-differentiation in the early stage since BFP-1 functioned at a concentration of $1 \, \mu g \, mL^{-1}$ [32]. Such burst release of pep-RA might not form the niche and could

not give the cells sustained osteo-differentiation stimulation. Although all the pep@MSNs-RA groups had a similar release profile, the delivered peptide amounts were different. The 1.0pep@MSNs-RA was screened for further in vitro study due to its ideal delivery performance on the 4th day ($1.09 \pm 0.04 \, \mu g \, mL^{-1}$) (Table S3). In short, the 1.0pep@MSNs-RA evaluated in subsequent cell experiments was referred to as pep@MSNs-RA. Thus, the in vitro release of pep@MSNs-RA suggested successful formation of a smart cell culture system with sustained drug delivery performance in the appropriate growth stage upon demand, and the initial osteo-inducing time might be on the 4th day. More importantly, the function time of the sequential delivered factor (BFP-1) could be initiated simply by regulating the pep@MSNs concentration in gels.
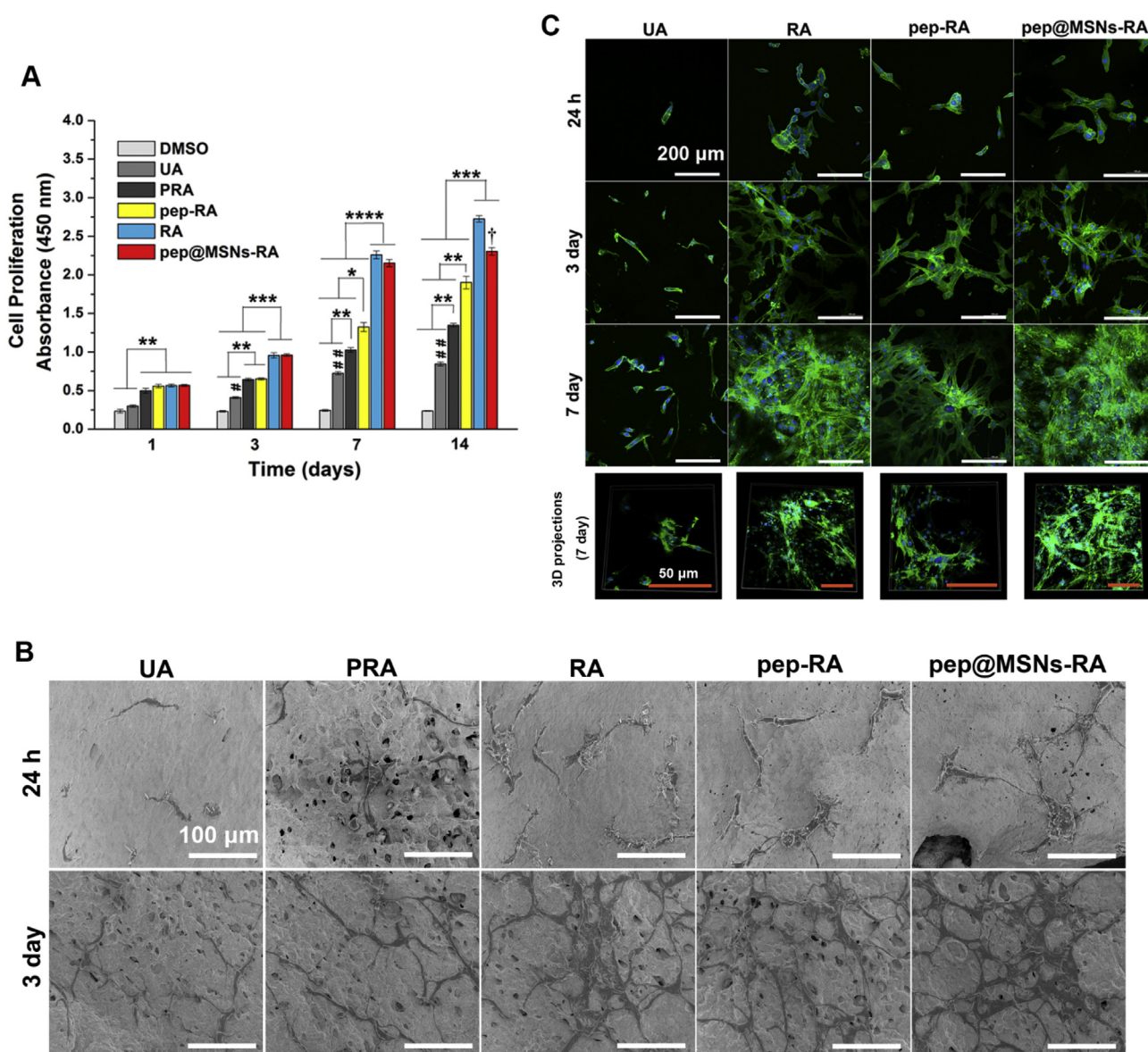

Fig. 5. The morphology and spreading of hMSCs cultured on the surface of different 2D substrates. A) Proliferation of hMSCs 3D cultured in different matrixes for 1, 3, 7 and 14 days. B) SEM images of hMSCs grown on different samples for 1 and 3 days. C) Adhesion morphology and F-actin cytoskeletal organization (green, labeled with FITC-phalloidin, counterstained with DAPI for nuclei in blue) of hMSCs after growth on UA, RA, pep-RA, and pep@MSNs-RA surface for 1, 3, and 7 days. Bottom: CLSM 3D projection images for F-actin and nuclei of hMSCs after cultured in various matrixes for 7 days. The p values were calculated by Tukey's post-hoc test ($^*p < 0.05$, $^{**}p < 0.01$, $^{***}p < 0.001$, and $^{****}p < 0.0001$; $\dagger p < 0.01$, relative to pep-RA and pep@MSNs-RA). All data represent mean $\pm$ SD ($n = 3$). (For interpretation of the references to color in this figure legend, the reader is referred to the Web version of this article.)

3.3. Survival and proliferation of hMSCs encapsulated in pep@MSNs-RA

In the design of pep@MSNs-RA, cell activity of hMSCs could be enhanced by the RGD bonded alginate hydrogel first and osteo-differentiation would then be sequentially induced by BFP-1 (Fig. 4A). Thus, the effects of pep@MSNs-RA on the survival and proliferation of hMSCs were investigated. Fig. 4B showed the CCK-8 results of cells encapsulated in UA, RA, PRA, pep-RA and pep@MSNs-RA for 1, 3, 7 and 14 days, suggesting that no alginate hydrogels had cytotoxicity. However, the cells grown in RA based gels showed outstanding cell viability compared with UA at each time point, while the cells in the PRA group showed poor activity. Live/dead staining results (Fig. 4C) showed that RA and pep@MSNs-RA induced little death after 5 days of culture, whereas almost all of the cells in UA and half the cells in PRA were killed. Cell proliferation is an event following cell adhesion [14,15], while alginate is a flexible polymer that does not present any cell adhesion ligands. Peptides including the RGD sequence have been extensively used to promote cell adhesion, as the presence of integrin receptors (e.g., $\alpha_v\beta_3$, $\alpha_5\beta_1$) for this ligand on is widespread on various cell types [46,47]. As the immunofluorescence staining for a universal cell adhesion receptor (integrin β1) in Fig. 4D, hMSCs cultured in RGD-treated gels expressed a high level of integrin β1. Hence, owing to the presence of the RGD peptide, the amount of cells in RA-based matrixes was higher than that on UA. Dramatically, among the RA based gels, PRA and pep-RA showed significantly lower cell viability than the other two groups (RA and pep@MSNs-RA) after 3 days of culture. Low proliferative potential often suggests a switch to differentiation [48], which could be the result of the potent osteo-stimulation from BFP-1 in the early proliferation stage. Combined with the release results in Table S3, the concentration of released BFP-1 from pep-RA was $1.12 \pm 0.04\,\mu g\,mL^{-1}$ on the first day, a concentration that could induce osteo-differentiation. Nevertheless, cell viability in the PRA group was lower than in the pep-RA group after 7 days of culture, which was due to the long-term osteo-stimulation from the grafted BFP-1 in PRA, slowing the proliferation rate. The bright-field images of hMSCs cultured in these matrixes (Fig. 4E) supported the hypothesis, where the size of cell clusters in RA and pep@MSNs-RA was much larger than that in PRA and pep-RA after cultured for 7 days. The above results suggest that the survivability and expansion of cells cultivated in pep@MSNs-RA were promoted.

3.4. Adhesion and spreading of hMSCs cultured with pep@MSNs-RA

The effects of pep@MSNs-RA on hMSCs adhesion and spreading in different culture system dimensions were investigated. As the CCK-8 and scanning electron microscope (SEM) images in Fig. 5A and B shown, more cells with better adhesion and spreading, compared with that of UA and PRA counterparts, were observed in the other three groups. Strikingly, hMSCs exhibited extended morphology with more pseudopodia on the 2D surface of RA, pep-RA, and pep@MSNs-RA (Fig. 5B). Otherwise, the thinner cell morphology was caused by the poor adhesion of UA, which agreed with the CCK-8 assay results (Fig. 5A). To further study the interaction between cells and substrates, the cytoskeleton (F-actin) of hMSCs grown on the matrixes was imaged. Fig. 5C showed distinct cell-cell contacts on all RA based gels after 3 days of culture, and these cells exhibited better growth in terms of the initial amounts and morphologies after seeding for 24 h. Moreover, limited spreading and filamentous morphology on UA were observed after culturing for 3 or 7 days, while cells cultured on RA based gels extended more adhering filopodia and spread to a greater extent with visible presentation of more mature F-actin

intracellular stress fibers. Importantly, no obvious difference was observed in RA, pep-RA and pep@MSNs-RA, indicating that the incorporated BFP-1 peptide could not have a positive impact on hMSCs adhesion or spreading, which was confirmed in previous studies [49].

Most studies linking biomaterials to cell activity have only been studied in 2D models, while the more physiologically relevant 3D culture system is essential to evaluate a bio-scaffold [50–52]. As measured from CLSM micrographs of phalloidin-FITC stained samples, hMSCs encapsulated within RA-based gels exhibited significantly increased cell spreading. Strikingly, hMSCs cultured in RA-based gels showed a well-spread morphology with distinct F-actin stress fibers on day 3, whereas hMSCs encapsulated in UA and b-hMSCs encapsulated in pep@MSNs-RA had rounded cell morphology without any noticeable stress fibers (Fig. 6A and Fig. S6). Some root-like cortical F-actin stress fibers on hMSCs, formed by the cell-peptide crosslinking [36,45], were observed in RA-based gels after 3 days of culture (Fig. 6A). Such root-like structures provided more biomechanic or biochemical cues from the surrounding microenvironment to cells, enhancing the survivability, spreading and proliferation of hMSCs [17,18]. Moreover, cells with the root-like structure might capture more growth factors from the matrix through the additional cell-peptide cross-linked networks. Furthermore, CLSM 3D projection images (Fig. 6B) showed more and larger cell clusters in RA and pep@MSNs-RA than in pep-RA after 7 days of culture, demonstrating that the presence of osteo-stimulation in the initial proliferation stage could have a negative effect on the aggregation of hMSCs. The CLSM results confirmed that the RGD ligands promoted the adhesion of hMSCs, thereby enhancing the proliferation of cells.

3.5. ALP activity

Fig. 7A showed the illustration of the niches in different gels during the differentiation stage, and the osteo-differentiation of hMSCs cultured with these gels was studied. Typically, ALP is a calcium- and phosphate-binding protein and a phosphor-hydrolytic enzyme that plays a major role in bone mineralization and is considered a phenotypic marker for osteoblast cells [53]. As shown in Fig. 7B and C, higher ALP activity was observed in RA-based groups compared to the UA group, but the ALP activity was significantly increased in cells cultured with pep-RA and pep@MSNs-RA on day 7. The ALP staining of hMSCs encapsulated in different gels for 7 days (Fig. 7D) confirmed these findings, where the cell clusters with a darker color were found in pep-RA and pep@MSNs-RA groups. Furthermore, the size of the cell clusters in pep-RA was smaller than in RA and pep@MSNs-RA, which was in accordance with the results of the cell activity study. The hMSCs in pep-RA were induced to differentiate during the initial period, which had a negative effect on cellular proliferation and aggregation. In addition, there was much higher ALP activity in pep@MSNs-RA compared to the other three groups on day 14 in both 2D and 3D systems (Fig. 7B and C). Based on the previous results, the proliferation and aggregation of hMSCs in pep@MSNs-RA were occurred before BFP-1 was working, leading to more and larger cell aggregates in pep@MSNs-RA than in pep-RA. The ALP activity demonstrated that the delayed and sustained delivery of the osteogenesis factor following the cell expansion stage could further enhance the osteogenic response.

3.6. Osteo-related genes and proteins expression of hMSCs cultured with pep@MSNs-RA in vitro

The osteo-differentiation of hMSCs is accompanied by a cascade of intracellular changes in gene or protein expression. An in-depth
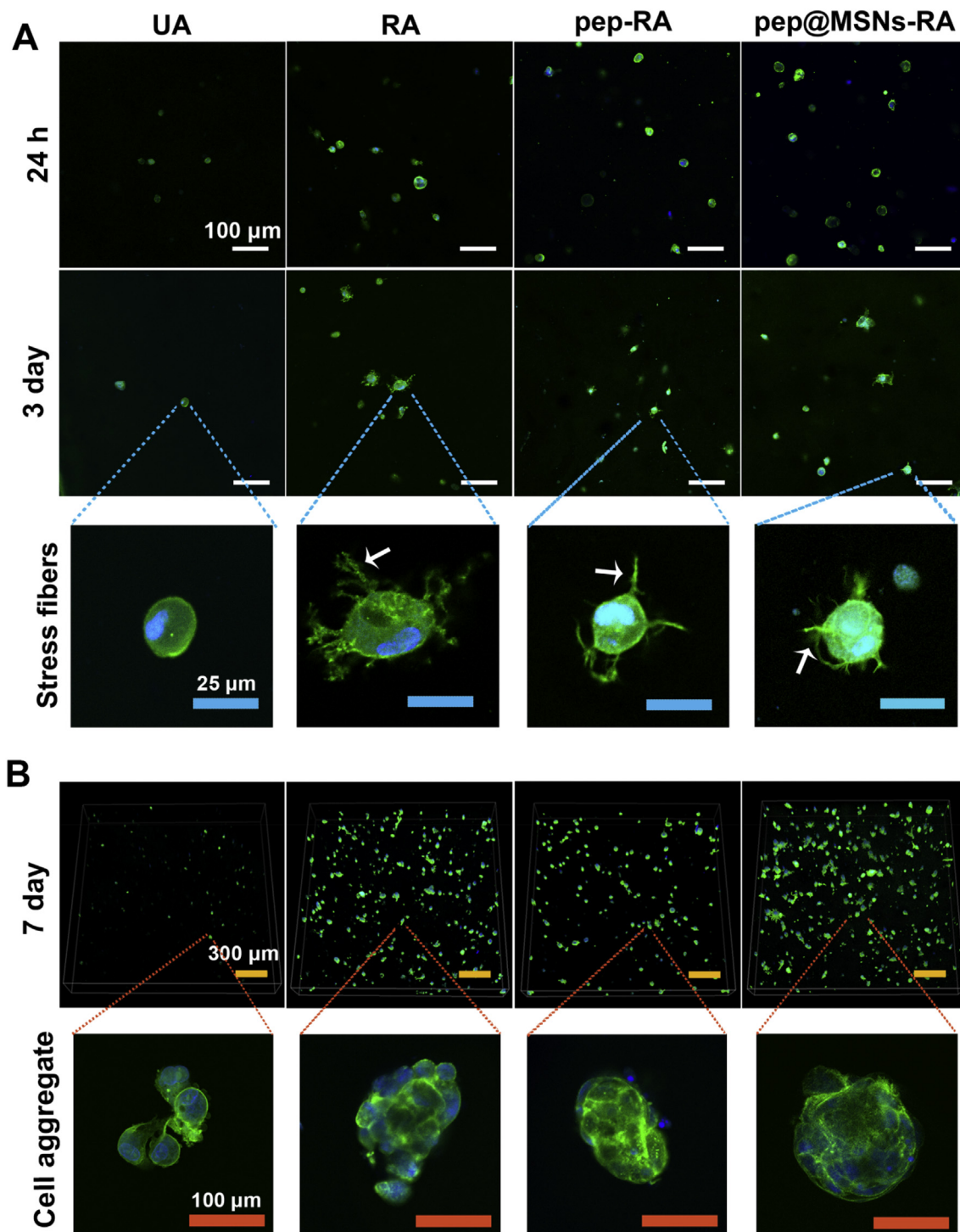
Fig. 6. *In situ* morphology of hMSCs encapsulated in different 3D matrixes. A) Morphology and F-actin cytoskeletal organization (green, labeled with FITC-phalloidin, counterstained with DAPI for nuclei in blue) of hMSCs after culture in UA, RA, pep-RA and pep@MSNs-RA for 1 and 3 days. B) CLSM 3D projection images for F-actin and nuclei of hMSCs and cell aggregates after culture in various matrixes for 7 days. (For interpretation of the references to color in this figure legend, the reader is referred to the Web version of this article.)

study of transcript levels was instrumental to revealing the cellular interactions with matrixes and their subsequent effect on various cell functions related to osteogenesis. Several studies using an RNA interference approach provided the evidence for the involvement of several genes (OCN, Col1a1, Runx2, etc.) in hMSCs-mediated osteo-differentiation. Q-PCR experiments were carried out to analyze osteo-specific gene expression from hMSCs cultured with UA, RA, pep-RA and pep@MSNs-RA at 7 or 14 days. As expected, the osteoblast specific genes of hMSCs encapsulated in RA, pep-RA, or pep@MSNs-RA, including ALP, OCN, Col1a1, and Runx2 (primers shown in Table S2), were upregulated compared to the UA group (Fig. 8A–D). Nevertheless, the genes in the pep@MSNs-RA group showed the highest expression, suggesting that the stimulation of this system on osteo-differentiation was greater than the other
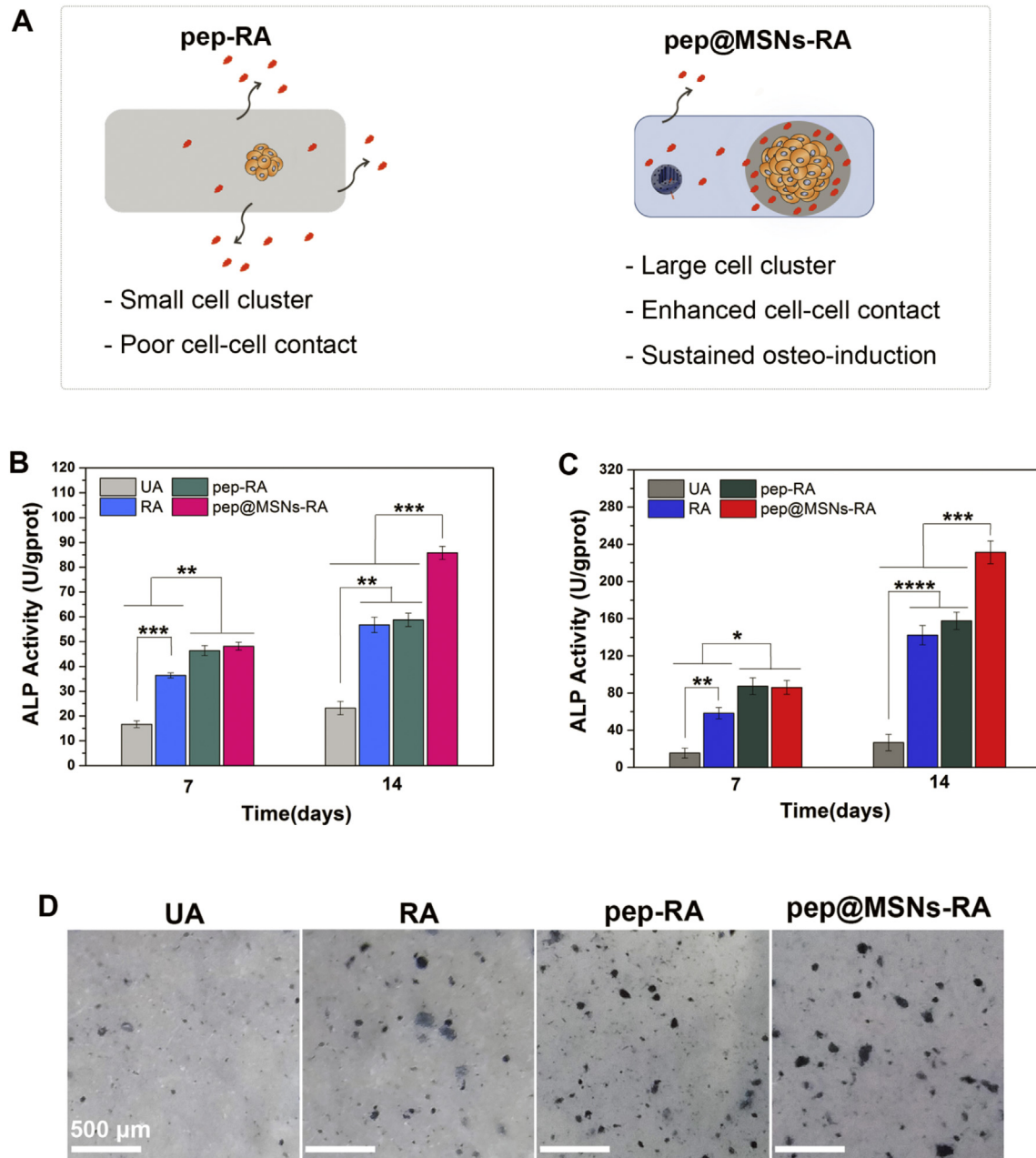
Fig. 7. The ALP activity of hMSCs in both 2D and 3D culture system. A) Illustration of the niches in pep-RA and pep@MSNs-RA during the osteo-differentiation stage. The effect of different matrixes on ALP activity of hMSCs B) on different 2D matrixes surface, or C) in different 3D gels. D) *In situ* staining for ALP activity (blue, BCIP/NBT) of hMSCs in different 3D matrixes at day 7. The p values were calculated by Tukey's post-hoc test (*$p < 0.05$, **$p < 0.01$, ***$p < 0.001$, and ****$p < 0.0001$). All data represent mean ± SD ($n = 3$). (For interpretation of the references to color in this figure legend, the reader is referred to the Web version of this article.)

groups. Particularly, when hMSCs were grown on 2D pep@MSNs-RA for 7 and 14 days, Runx2 showed 2.8-fold and 15.8-fold upregulation, respectively (Fig. 8A). Runx2 plays a vital role in regulating both embryonic bone development and postnatal osteoblastic function. Moreover, Runx2 expression can stimulate the differentiation of MSCs to differentiate into osteoblasts and inhibit their differentiation into chondrocytes and adipocytes [53], as well as upregulate the expression of bone matrix genes (OCN, Col1a1, etc.). Strikingly, OCN showed the highest increase (132.6-fold) when hMSCs were cultured on pep@MSNs-RA for 14 days (Fig. 8B). Of all the osteo-related genes, OCN is expressed in differentiating cells and is the most specific gene for mineralization and osteoblast differentiation. It reaches maximum expression during

mineralization and accumulates in the mineralized bone [54]. Furthermore, the expression of Col1a1 when hMSCs were cultivated on the pep@MSNs-RA significantly outmatched those on pep-RA and RA on day 7 or 14 (Fig. 8C). Col1a1 is the most abundant protein of the extracellular bone matrix and has an important role in influencing cellular behavior [55]. The bioactivity in osteo-differentiation of pep@MSNs-RA could be due to the BFP-1 delivered by pep@MSNs at the right time. As mentioned above, BFP-1 derived from BMP-7 protein exhibits an improved osteogenic induction property, and may bind to the same functional sites (BMP receptors) and induce the upregulation of target bone-related genes through Smads or mitogen-activated protein kinase (MAPK) [33]. Moreover, the BFP-1 captured by cell-crosslinked
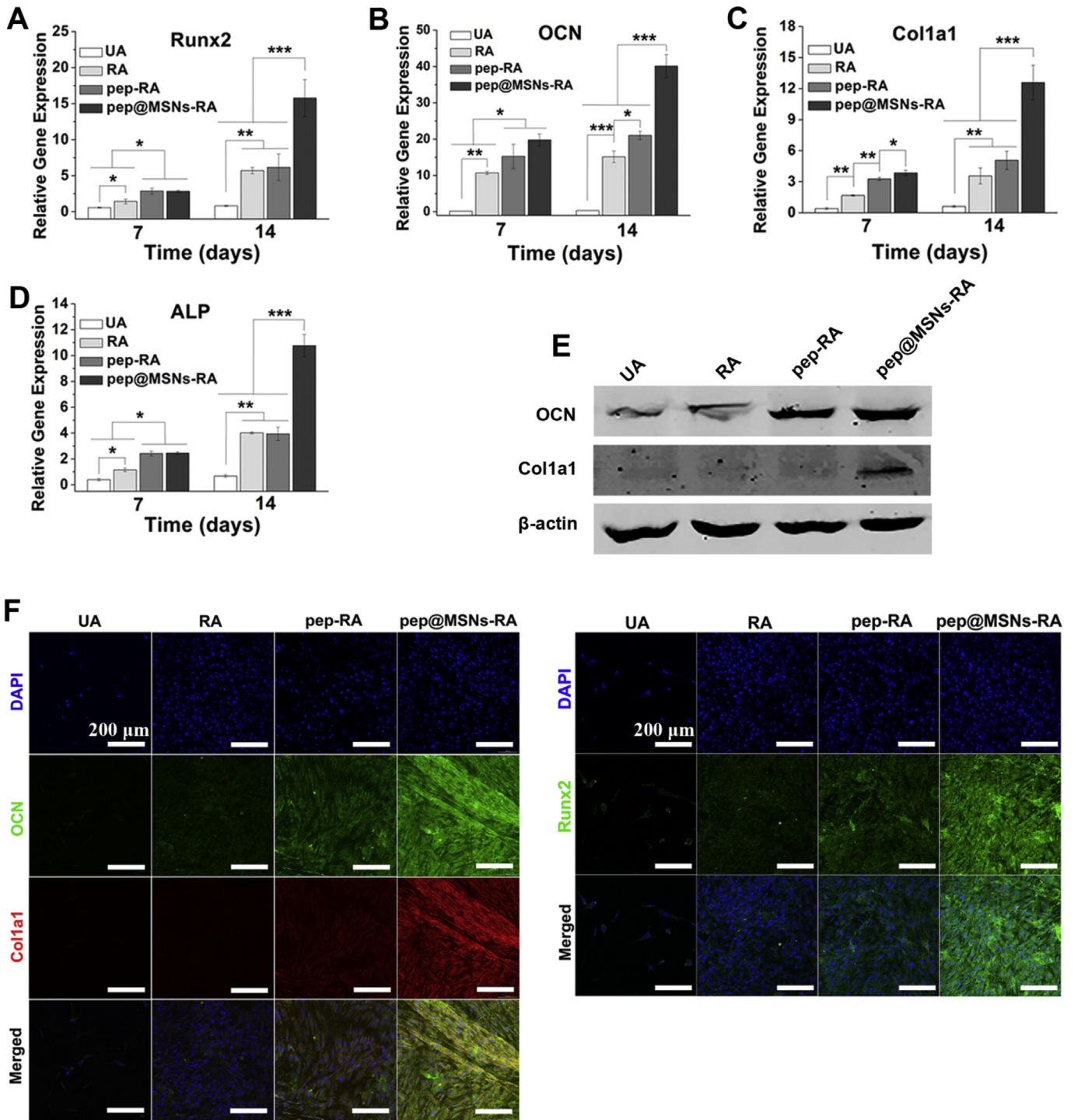
Fig. 8. The effect of different matrixes on osteo-related gene and protein expression of hMSCs in a 2D culture system. (A—D) Q-PCR analysis for osteo-related genes in hMSCs, including OCN, Col1a1, Runx2, and ALP. E) Western blot analysis of OCN and Col1a1 expression in hMSCs at day 14. F) *In situ* immunofluorescence staining for OCN (green), Col1a1 (red), Runx2 (green), and nuclear counterstain DAPI (blue) at day 14. The *p* values were calculated by Tukey's post-hoc test (*$p < 0.05$, **$p < 0.01$, and ***$p < 0.001$). All data represent mean $\pm$ SD ($n = 3$). (For interpretation of the references to color in this figure legend, the reader is referred to the Web version of this article.)

networks in pep@MSNs-RA led to sustained osteo-stimulation after the proliferation stage. The results confirmed the hypothesis that independent and sequential stimulation in proliferation and osteogenesis stages could synergistically enhance osteo-differentiation of hMSCs.

Interestingly, when hMSCs were encapsulated in 3D matrixes,

osteogenesis-related gene expression (OCN, Col1a1, Runx2 and ALP) significantly outmatched those on the 2D pep@MSNs-RA surface at both day 7 and 14 (Fig. 9A—D). Based on the above results, hMSCs encapsulated in 3D gels could capture more BFP-1 from the surrounding microenvironment by the root-like structures. In addition, the previous studies demonstrated the number of
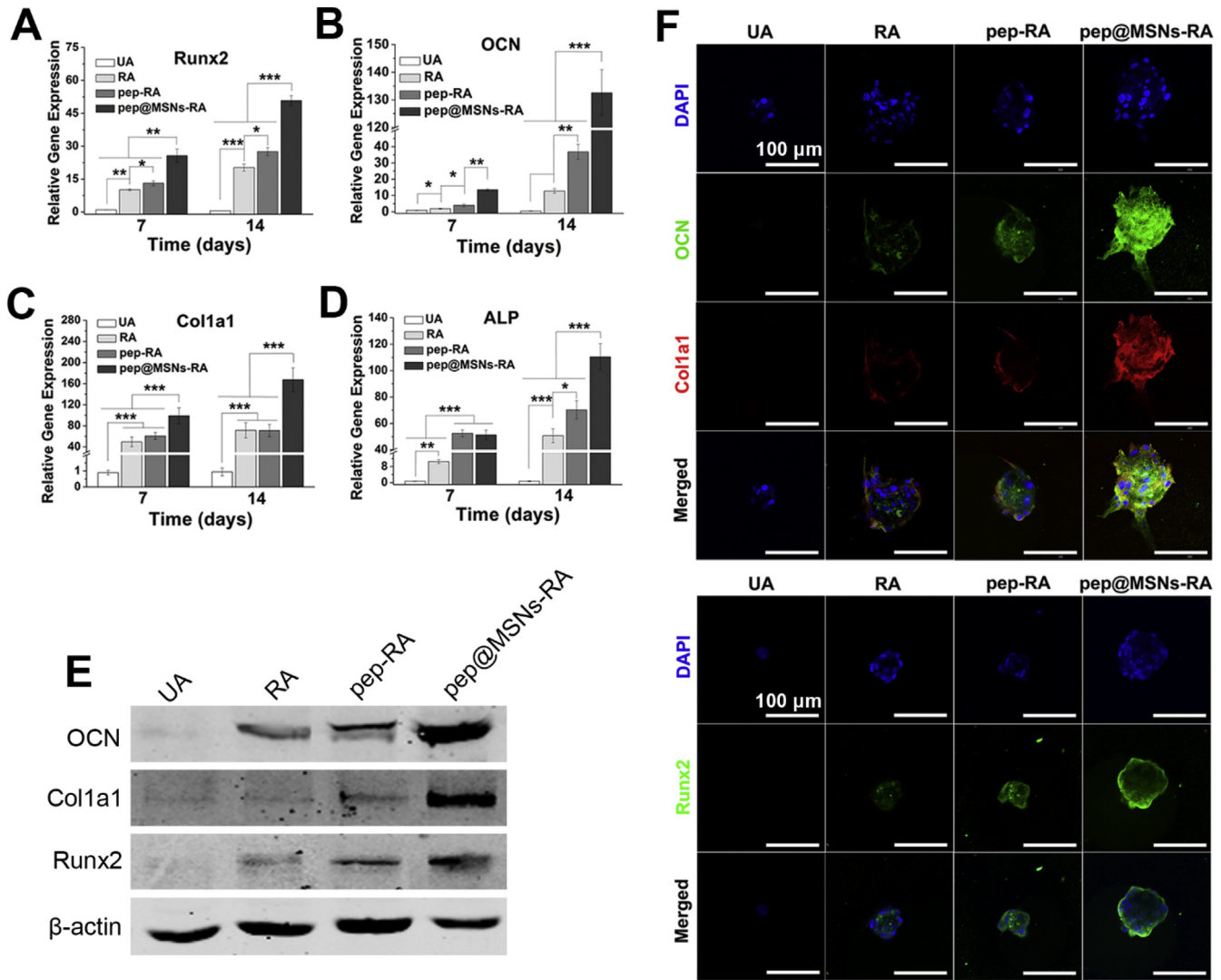
Fig. 9. Osteo-related gene and protein expression in hMSCs cultured in different 3D gels. (A–D) Q-PCR analysis for osteo-related genes in hMSCs, including OCN, Col1a1, Runx2, and ALP. E) Western blot analysis of OCN, Col1a1, and Runx2 expression in hMSCs at day 14. F) *In situ* immunofluorescence staining for OCN (green), Col1a1 (red), Runx2 (green), and nuclear counterstain DAPI (blue) at day 14. The *p* values were calculated by Tukey's post-hoc test (*$p < 0.05$, **$p < 0.01$, and ***$p < 0.001$). All data represent mean ± SD ($n = 3$). (For interpretation of the references to color in this figure legend, the reader is referred to the Web version of this article.)

MSCs osteo-differentiation based on the extent of cell-cell contact, and the extent of osteo-differentiation was fairly linearly related to the extent of neighboring cells [16]. Clearly, the formation of cell clusters would enhance the cell-cell contact, and the hMSCs cultivated in 3D matrixes might prefer to aggregate.

Though the osteo-related gene expression in the pep@MSNs-RA groups were improved at day 7 and 14, the protein level needed to be assessed. Thus, immunofluorescence staining and Western blotting were utilized to further validate the expression of the osteo-related proteins at the translational level. Western blotting of key osteogenic proteins involved in initial (Col1a1) and mid-to-late (OCN) stage showed clear band expressions of both proteins in pep@MSNs-RA (Figs. 8E and 9E). The expression of Col1a1 and OCN in pep@MSNs-RA was clearly higher than that of the other three groups, corresponding to the gene analysis findings. The delivered and sustained osteo-stimulation by BFP-1 significantly increased the expression of the osteogenic proteins. Furthermore, the immunochemical staining of cells qualitatively supports the protein production results (Figs. 8F and 9F, Fig. S7 and S8). In addition, the current data supported the hypothesis that the cell aggregates in

the 3D matrixes, in comparison with the 2D system, could induce osteo-differentiation to a greater extent. Owing to the enhanced expansion of the hMSCs encapsulated in RA-based gels, the cells aggregated together and formed cell clusters in RA, pep-RA, and pep@MSNs-RA matrixes (Fig. 9F). The expression level of all osteo-related proteins in hMSCs had a higher upregulation in pep@MSNs-RA than those in pep-RA after 14 days. Typically, the significantly high secretion of osteogenic proteins indicated that pep@MSNs-RA possessed the potential to provide a niche for hMSCs to mineralize and grow into the mature bone tissue.

3.7. Osteogenesis of hMSCs encapsulated in pep@MSNs-RA in vivo

To examine the bone matrix deposition and mineralization in hMSCs-loaded pep@MSNs-RA, various gels (including UA, RA, pep-RA and pep@MSNs-RA) encapsulated with hMSCs were subcutaneously implanted into nude mice (Fig. 10A). Fig. 10B showed the gross view of different hMSCs-loaded matrixes that remove from the mice at 2 and 4 weeks post-implantation. Combined with the H&E and MT staining results (Fig. 11A), thin
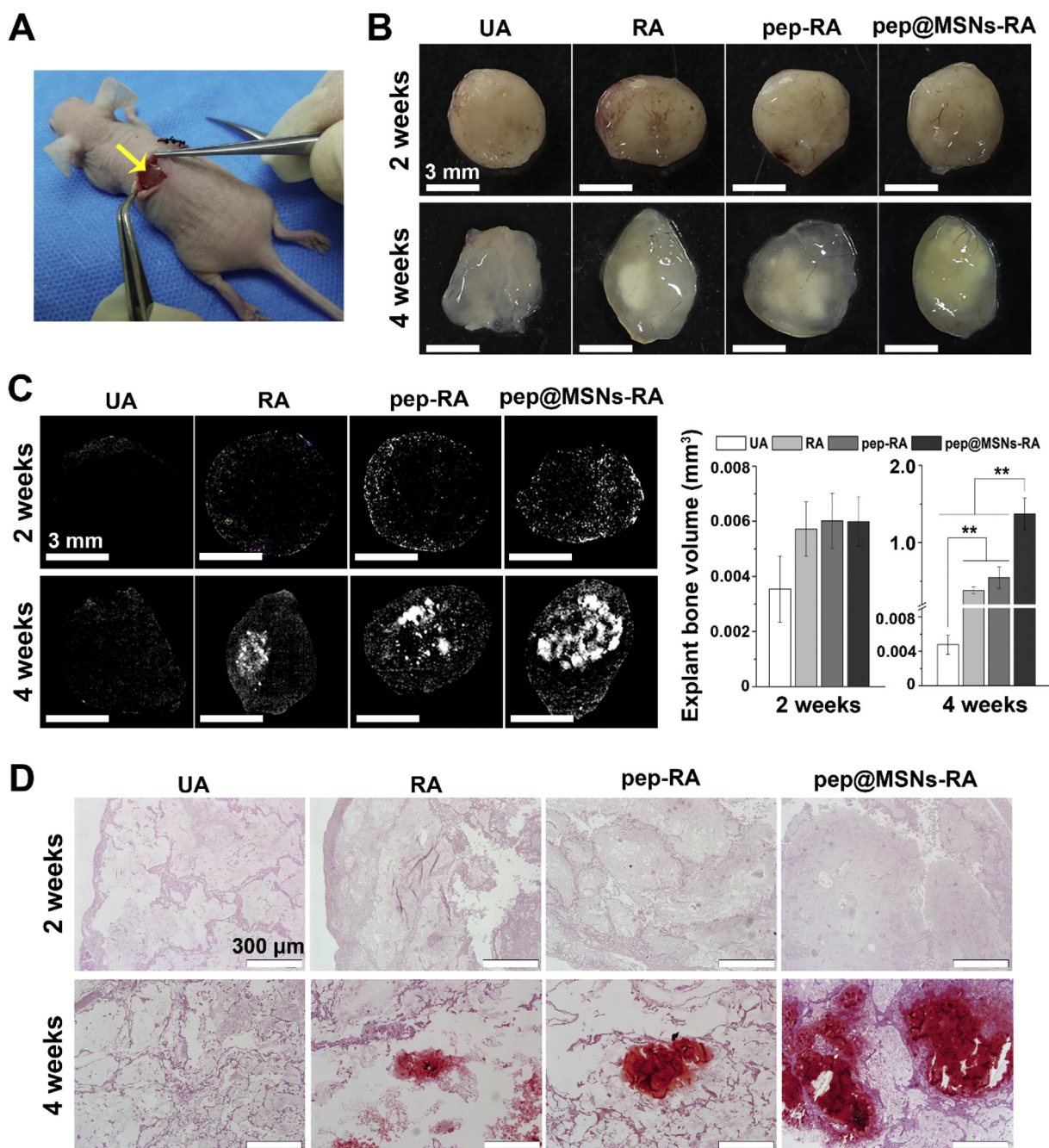
Fig. 10. Visualized gross view and quantified volume of mineralized matrix in different hMSCs-loaded gels *in vivo*. A) Gels encapsulated with hMSCs were subcutaneously implanted into nude mice. B) Gross view of different hMSCs-loaded gels following removal from mice 2 and 4 weeks post surgery. C) Micro-CT reconstruction images of gels mineralization and quantitative bone volume analysis after 2 and 4 weeks of implantation. D) Alizarin Red-S (ARS) staining of the implanted hMSCs-loaded gels after 2 and 4 weeks of subcutaneous implantation. The *p* values were calculated by Tukey's post-hoc test (**$p < 0.01$). All data represent mean $\pm$ SD ($n = 3$). (For interpretation of the references to color in this figure legend, the reader is referred to the Web version of this article.)

fibrous capsule layers with some blood vessels, unavoidable upon biomaterials implantation caused by foreign body response [56], were observed around all the matrixes at 2 weeks. However, almost no fibrous layers were found on all matrixes surface at 4 weeks, due to the good biocompatibility of alginate. Moreover, visible and abundant blood vessels were observed on the surface and inside of the RA, pep-RA, and pep@MSNs-RA (Figs. 10B and 11A), indicating the favorable blood vessels ingrowth of RA based gels. In addition, the micro-CT analysis results in Fig. 10C showed the visualized new bone tissue distribution and

quantitative bone volume, and there were little mineralization occurring in any groups at 2 weeks. Nevertheless, RA, pep-RA, and pep@MSNs-RA groups exhibited mineralization inside of the gels at 4 weeks, and much more mineralized bone tissue were found in pep@MSNs-RA groups (Fig. 10C). Histological sections analysis of implants stained with ARS (Fig. 10D) and MT (Fig. 11A) supported the micro-CT analysis. Cross-sectional images of hMSCs-loaded UA stained by ARS exhibited no mineral deposition at 2 and 4 weeks. However, mineralized calcium deposits were observed in hMSCs-loaded RA based gels (containing RA, pep-RA, and
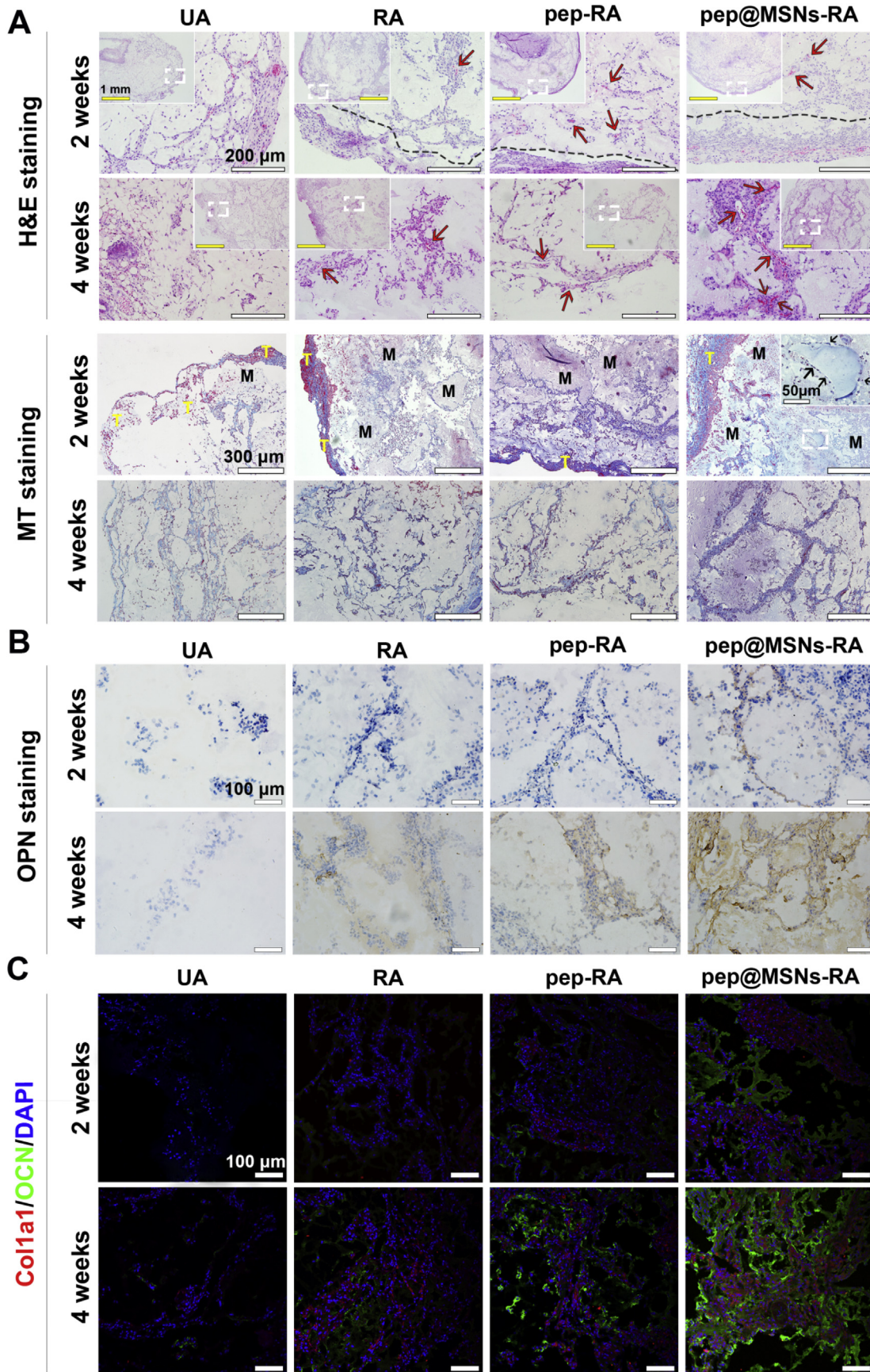
Fig. 11. Histological analysis for the hMSCs-loaded gels after 2 and 4 weeks of implantation *in vivo*. A) H&E and MT staining (dashed lines: borders between gels and host tissues; red arrows: blood vessels; black arrows: osteoblast-like cells at the edge of newly forming tissue; M: matrix gels; T: host tissues), B) IHC staining against OPN, C) IF staining against Col1a1 (red) and OCN (green) of the hMSCs-loaded gels after 2 and 4 weeks of subcutaneous implantation. (For interpretation of the references to color in this figure legend, the reader is referred to the Web version of this article.)

pep@MSNs-RA) and much more mineralization occurred in pep@MSNs-RA groups at 4 weeks. MT staining images showed some osteoid forming at 2 weeks and more collagen deposition at 4 weeks in hMSCs-loaded pep@MSNs-RA.

To further evaluate the *in vivo* osteo-differentiation of hMSCs encapsulated in the gels, the osteo-related proteins were monitored by a set of immunohistological analysis at 2 and 4 weeks post-implantation. ICH and IF staining (Fig. 11B and C, Fig. S9) results indicated that OPN, OCN, and Col1a1 were detected in RA, pep-RA, and pep@MSNs-RA groups at 4 weeks post-implantation. Significantly, both OPN and OCN, two important osteogenic markers, were much highly expressed by hMSCs in pep@MSNs-RA than those in the other three groups at 2 and 4 weeks. Such favorable *in vivo* mineralization and osteo-differentiation of hMSCs encapsulated in pep@MSNs-RA were attributed to the delayed and sustained delivery of BFP-1, which was in accordance with the above *in vitro* findings. Thus, all the results had confirmed the hypothesis that the sequentially independent stimulation in the proliferation and differentiation stages could significantly promote the survivability, expansion, and osteo-differentiation of hMSCs in the time-responsive osteogenic niche.

4. Conclusions

pep@MSNs-RA was successfully prepared by a peptide-laden, nanocarrier-encapsulated, alginate-based hydrogel matrix as a versatile cell culture system with the ability to independently deliver multiple growth factors at the appropriate stages. Using the system, the activity (including survivability, spreading, expansion and aggregation) of hMSCs was promoted by an adhesion ligand (RGD)-modified alginate matrix at an early stage, and pep@MSNs would deliver an osteogenic factor (BFP-1) to induce osteo-differentiation after cell spreading and expansion. Moreover, the starting time of osteo-induction could be simply regulated by changing the concentration of the encapsulated pep@MSNs. The mechanical integrity of gels and sustained-released performance of BFP-1 were enhanced in the hMSCs-loaded pep@MSNs-RA, due to the additional cell-peptide cross-linked networks. Furthermore, pep@MSNs-RA was effective in stimulating hMSCs proliferation and accelerating the formation of cell aggregates as early as 7 days. The osteo-induction was initiated after cell expansion and sustained for a long time, leading to the rapid formation of bone matrix and mineralized bone tissues. Broadly, this versatile and injectable system sufficient for stem cell survival and fate control could be useful for tissue regeneration and 3D bio-printing.

Acknowledgements

Appendix A. Supplementary data

Supplementary data related to this article can be found at https://doi.org/10.1016/j.biomaterials.2018.02.025.

References

[1] J. Park, I.Y. Kim, M. Patel, H.J. Moon, S.J. Hwang, B. Jeong, 2D and 3D hybrid systems for enhancement of chondrogenic differentiation of tonsil-derived mesenchymal stem cells, Adv. Funct. Mater. 25 (2015) 2573—2582.

[2] J.M. Grichnik, J.A. Burch, R.D. Schulteis, S. Shan, J. Liu, T.L. Darrow, C.E. Vervaert, H.F. Seigler, Melanoma, a tumor based on a mutant stem cell, J. Invest. Dermatol. 126 (2006) 142—153.

[3] I. Bozic, M.A. Nowak, Unwanted evolution, Science 342 (2013) 938—939.

[4] M.P. Lutolf, P.M. Gilbert, H.M. Blau, Designing materials to direct stem-cell fate, Nature 462 (2009) 433—441.

[5] B. Tabisz, W. Schmitz, M. Schmitz, T. Luehmann, E. Heusler, J.C. Rybak, L. Meinel, J.E. Fiebig, T.D. Mueller, J. Nicke, Site-directed immobilization of BMP-2: two approaches for the production of innovative osteoinductive scaffolds, Biomacromolecules 18 (2017) 695—708.

[6] E. Dawson, G. Mapili, K. Erickson, S. Taqvi, K. Roy, Biomaterials for stem cell differentiation, Adv. Drug Deliv. Rev. 60 (2008) 215—228.

[7] O.F. Zouani, C. Chanseau, B. Brouillaud, R. Bareille, F. Deliane, M.-P. Foulc, A. Mehdi, M.-C. Durrieu, Altered nanofeature size dictates stem cell differentiation, J. Cell Sci. 125 (2012) 1217—1224.

[8] S. Watari, K. Hayashi, J.A. Wood, P. Russell, P.F. Nealey, C.J. Murphy, D.C. Genetos, Modulation of osteogenic differentiation in hMSCs cells by submicron topographically-patterned ridges and grooves, Biomaterials 33 (2012) 128—136.

[9] A.J. Engler, S. Sen, H.L. Sweeney, D.E. Discher, Matrix elasticity directs stem cell lineage specification, Cell 126 (2006) 677—689.

[10] J.M. Wozney, V.R. Anthony, J. Celeste, L.M. Mitsock, M.J. Whitters, R.W. Kriz, Novel regulators of bone formation: molecular clones and activities, Science 242 (1988) 1528—1535.

[11] S. Park, M. Park, B.H. Kim, J.E. Lee, H.J. Park, S.H. Lee, C.Y. Heo, Y.H. Chan, Acute suppression of TGF-ß with local, sustained release of tranilast against the formation of fibrous capsules around silicone implants, J. Contr. Release 200 (2015) 125—137.

[12] S.-L. Cheng, J.W. Yang, L. Rifas, S.-F. Zhang, L.V. Avioli, Differentiation of human bone marrow osteogenic stromal cells *in vitro*: induction of the osteoblast phenotype by dexamethasone, Endocrinology 134 (1994) 277—286.

[13] B. Tabisz, W. Schmitz, M. Schmitz, T. Luehmann, H. Eva, J.C. Rybak, Site-directed immobilization of BMP-2: two approaches for the production of innovative osteoinductive Scaffolds, Biomacromolecules 18 (2017) 695—708.

[14] A.R. Costa-Pinto, A.J. Salgado, V.M. Correlo, P. Sol, M. Bhattacharya, P. Charbord, R.L. Reis, N.M. Neves, Adhesion, proliferation, and osteogenic differentiation of a mouse mesenchymal stem cell line (BMC9) seeded on novel melt-based chitosan/polyester 3D porous scaffolds, Tissue Eng. 14 (2008) 1049—1057.

[15] P.Y. Wang, L.R. Clements, H. Thissen, A. Jane, W.B. Tsai, N.H. Voelcker, Screening mesenchymal stem cell attachment and differentiation on porous silicon gradients, Adv. Funct. Mater. 22 (2012) 3414—3423.

[16] J. Tang, R. Peng, J. Ding, The regulation of stem cell differentiation by cell-cell contact on micropatterned material surfaces, Biomaterials 31 (2010) 2470—2476.

[17] T.H. Qazi, D.J. Mooney, G.N. Duda, S. Geissler, Biomaterials that promote cell-cell interactions enhance the paracrine function of MSCs, Biomaterials 140 (2017) 103—114.

[18] K.E. Kasza, A.C. Rowat, J. Liu, T.E. Angelini, C.P. Brangwynne, G.H. Koenderink, D.A. Weitz, The cell as a material, Curr. Opin. Cell Biol. 19 (2007) 101—107.

[19] A.S. Mao, J.W. Shin, D.J. Mooney, Effects of substrate stiffness and cell-cell contact on mesenchymal stem cell differentiation, Biomaterials 98 (2016) 184.

[20] T.P. Richardson, M.C. Peters, A.B. Ennett, D.J. Mooney, Polymeric system for dual growth factor delivery, Nat. Biotechnol. 19 (2001) 1029—1034.

[21] D.S. Benoit, S.D. Collins, K.S. Anseth, Multifunctional hydrogels that promote osteogenic human mesenchymal stem cell differentiation through stimulation and sequestering of bone morphogenic protein 2, Adv. Funct. Mater. 17 (2007) 2085—2093.

[22] T.P. Richardson, M.C. Peters, A.B. Ennett, D.J. Mooney, Polymeric system for dual growth factor delivery, Nat. Biotechnol. 19 (2001) 1029—1034.

[23] M. Wang, Y. Deng, P. Zhou, Z. Luo, Q. Li, B. Xie, X. Zhang, T. Chen, D. Pei, Z. Tang, *In vitro* culture and directed osteogenic differentiation of human pluripotent stem cells on peptides-decorated two-dimensional microenvironment, ACS Appl. Mater. Interfaces 7 (2015) 4560—4572.

[24] C. Dai, H. Guo, J. Lu, J. Shi, J. Wei, C. Liu, Osteogenic evaluation of calcium/magnesium-doped mesoporous silica scaffold with incorporation of rhBMP-2 by synchrotron radiation-based μCT, Biomaterials 32 (2011) 8506—8517.

[25] S. Chen, J. Yang, H. Wang, Y. Chao, C. Zhang, J. Shen, P. Zhang, Adenovirus encoding BMP-7 immobilized on titanium surface exhibits local delivery ability and regulates osteoblast differentiation in vitro, Arch. Oral Boil. 58 (2013) 1225—1231.

[26] K.Y. Lee, D.J. Mooney, Alginate: properties and biomedical applications, Prog. Polym. Sci. 37 (2012) 106—126.

[27] R.S. Stilhano, J.L. Madrigal, K.P. Wong, A. Williams, P.K. Martin, F.S.M. Yamaguchi, V.Y. Samoto, S.W. Han, Injectable alginate hydrogel for enhanced spatiotemporal control of lentivector delivery in murine skeletal muscle, J. Contr. Release 237 (2016) 42—49.

[28] J.A. Rowley, G. Madlambayan, D.J. Mooney, Alginate hydrogels as synthetic extracellular matrix materials, Biomaterials 20 (1999) 45—53.

[29] J.A. Rowley, D.J. Mooney, Alginate type and RGD density control myoblast phenotype, J. Biomed. Mater. Res. 60 (2002) 217—223.

[30] R. Langer, D.A. Tirrell, Designing materials for biology and medicine, Nature 428 (2004) 487—492.

[31] Z. Luo, Y. Yang, Y. Deng, Y. Sun, H. Yang, S. Wei, Peptide-incorporated 3D porous alginate scaffolds with enhanced osteogenesis for bone tissue engineering, Colloids Surf. B Biointerfaces 143 (2016) 243—251.

[32] H.K. Kim, J.H. Kim, D.S. Park, K.S. Park, S.S. Kang, J.S. Lee, M.H. Jeong, T.R. Yoon, Osteogenesis induced by a bone forming peptide from the prodomain region

of BMP-7, Biomaterials 33 (2012) 7057—7063.

[33] Z. Luo, Y. Deng, R. Zhang, M. Wang, Y. Bai, Q. Zhao, Y. Lyu, J. Wei, S. Wei, Peptide-laden mesoporous silica nanoparticles with promoted bioactivity and osteo-differentiation ability for bone tissue engineering, Colloids Surf. B Biointerfaces 131 (2015) 73—82.

[34] Y. Zhang, Z. Zhi, T. Jiang, J. Zhang, Z. Wang, S. Wang, Spherical mesoporous silica nanoparticles for loading and release of the poorly water-soluble drug telmisartan, J. Contr. Release 145 (2010) 257—263.

[35] L. Palanikumar, H.Y. Kim, J.Y. Oh, A.P. Thomas, E.S. Choi, M.T. Jeena, S.H. Joo, J.H. Ryu, Noncovalent surface locking of mesoporous silica nanoparticles for exceptionally high hydrophobic drug loading and enhanced colloidal stability, Biomacromolecules 16 (2015) 2701—2714.

[36] K.Y. Lee, H.J. Kong, R.G. Larson, D.J. Mooney, Hydrogel formation via cell crosslinking, Adv. Mater. 21 (2003) 1828—1832.

[37] N. Huebsch, E. Lippens, K. Lee, M. Mehta, S.T. Koshy, M.C. Darnell, R.M. Desai, C.M. Madl, M. Xu, X. Zhao, Matrix elasticity of void-forming hydrogels controls transplanted-stem-cell-mediated bone formation, Nat. Mater. 14 (2015) 1269—1277.

[38] O. Chaudhuri, S.T. Koshy, C.B. da Cunha, J.-W. Shin, C.S. Verbeke, K.H. Allison, D.J. Mooney, Extracellular matrix stiffness and composition jointly regulate the induction of malignant phenotypes in mammary epithelium, Nat. Mater. 13 (2014) 970—978.

[39] R.K. Das, V. Gocheva, R. Hammink, O.F. Zouani, A.E. Rowan, Stress-stiffening-mediated stem-cell commitment switch in soft responsive hydrogels, Nat. Mater. 15 (2016) 318—325.

[40] N. Huebsch, P.R. Arany, A.S. Mao, D. Shvartsman, O.A. Ali, S.A. Bencherif, J. Rivera-Feliciano, D.J. Mooney, Harnessing traction-mediated manipulation of the cell/matrix interface to control stem-cell fate, Nat. Mater. 9 (2010) 518—526.

[41] S. Maiti, K. Singha, S. Ray, P. Dey, B. Sa, Adipic acid dihydrazide treated partially oxidized alginate beads for sustained oral delivery of flurbiprofen, Pharmaceut. Dev. Technol. 14 (2009) 461—470.

[42] A. Xu, L. Zhou, Y. Deng, X. Chen, X. Xiong, F. Deng, S. Wei, A carboxymethyl chitosan and peptide-decorated polyetheretherketone ternary biocomposite with enhanced antibacterial activity and osseointegration as orthopedic/dental implants, J. Mater. Chem. B Mater. Biol. Med. 4 (2016) 1878—1890.

[43] E. Eteshola, L.J. Brillson, S.C. Lee, Selection and characteristics of peptides that bind thermally grown silicon dioxide films, Biomol. Eng. 22 (2005) 201—204.

[44] V. Puddu, C.C. Perry, Peptide adsorption on silica nanoparticles: evidence of hydrophobic interactions, ACS Nano 6 (2012) 6356—6363.

[45] J.L. Drury, T. Boontheekul, D.J. Mooney, Cellular cross-linking of peptide modified hydrogels, J. Biomech. Eng. 127 (2005) 220—228.

[46] P.P. Lehenkari, M.A. Horton, Single integrin molecule adhesion forces in intact cells measured by atomic force microscopy, Biochem. Biophys. Res. Commun. 259 (1999) 645—650.

[47] L.Y. Koo, D.J. Irvine, A.M. Mayes, D.A. Lauffenburger, L.G. Griffith, Co-regulation of cell adhesion by nanoscale RGD organization and mechanical stimulus, J. Cell Sci. 115 (2002) 1423—1433.

[48] C. Mahapatra, R.K. Singh, J.J. Kim, K.D. Patel, R.A. Perez, J.H. Jang, H.W. Kim, Osteopromoting reservoir of stem cells: bioactive mesoporous nanocarrier/collagen gel through slow-releasing FGF18 and the activated BMP signaling, ACS Appl. Mater. Interfaces 8 (2016) 27573—27584.

[49] Y.J. Lee, J.-H. Lee, H.-J. Cho, H.K. Kim, T.R. Yoon, H. Shin, Electrospun fibers immobilized with bone forming peptide-1 derived from BMP7 for guided bone regeneration, Biomaterials 34 (2013) 5059—5069.

[50] L.G. Griffith, M.A. Swartz, Capturing complex 3D tissue physiology in vitro, Nat. Rev. Mol. Cell Biol. 7 (2006) 211—224.

[51] E. Cukierman, R. Pankov, D.R. Stevens, K.M. Yamada, Taking cell-matrix adhesions to the third dimension, Science 294 (2001) 1708—1712.

[52] A. Arranja, A.G. Denkova, K. Morawska, G. Waton, S.P. Vlierberghe, F. Dubruel, E. Mendes, Interactions of pluronic nanocarriers with 2D and 3D cell cultures: effects of PEO block length and aggregation state, J. Contr. Release 224 (2016) 126—135.

[53] C. Zheng, J. Wang, Y. Liu, Q. Yu, Y. Liu, N. Deng, J. Liu, Functional selenium nanoparticles enhanced stem cell osteoblastic differentiation through BMP signaling pathways, Adv. Funct. Mater. 24 (2014) 6872—6883.

[54] G. Kaur, M.T. Valarmathi, J.D. Potts, Q. Wang, The promotion of osteoblastic differentiation of rat bone marrow stromal cells by a polyvalent plant mosaic virus, Biomaterials 29 (2008) 4074—4081.

[55] T. Lu, X. Liu, S. Qian, H. Cao, Y. Qiao, Y. Mei, P.K. Chu, C. Ding, Multilevel surface engineering of nanostructured TiO_2 on carbon-fiber-reinforced polyetheretherketone, Biomaterials 35 (2014) 5731—5740.

[56] J.M. Anderson, A. Rodriguez, D.T. Chang, Foreign body reaction to biomaterials, Semin. Immunol. 20 (2008) 86—100.